RUSSIAN JOURNAL OF EARTH SCIENCES, VOL. 3, NO. 4, PAGES 247–275, OCTOBER 2001

Modeling of seismo-electromagnetic phenomena

N. Gershenzon and G. Bambakidis

Department of Physics Wright State University, Dayton, Ohio U.S.A.

Abstract. A model for seismo-electromagnetic (SEM) phenomena is described. The electromagnetic signals generated by mechanical disturbances in the earths crust have been calculated and compared with reported seismo-electromagnetic signals (SEMS). The major known SEM phenomena, namely, tectonomagnetic variations, electrotelluric anomalies, geomagnetic variations in the ultra-low frequency range and electromagnetic emission in the radio frequency range, have been considered. We have calculated the spectral densities associated with various types of sources. The set of formulas necessary to calculate the detected (filtered and averaged) electric and magnetic fields generated by mechanical disturbances for a wide range of frequencies and at various distances from the source are presented. Based on these formulas, we discuss the conditions under which electrokinetic, piezomagnetic and piezolectric effects could be responsible for SEMS. A comparison of estimated values of SEMS with reported field measurements leads to the conclusion that the sources of most anomalous SEMS are relatively close to the detector. In other words, the source of the signal is local, although the source of the mechanical disturbance which activates it, i.e. the epicenter of an earthquake, may be far away. Recommendations for field experiments (appropriate detector sitting, detector parameters and frequency range) following from the model developed here are presented.

1. Introduction

Electromagnetic phenomena preceding and accompanying seismic events continue to attract attention not only as possible earthquake precursors but also as additional parameters for describing the earths crust and its dynamics. Before considering seismo-electromagnetic (SEM) phenomena, however, we address the question of whether such phenomena do in fact exist.

In spite of the publication of several hundred articles from the beginning of the twentieth century dealing with the relationship between EM signals and pre-seismic processes in the earths crust, there is still no definitive proof that the two are connected. While there are several reasons for this, we think that the main reason is the practical impossibility of repeating the results of field observations. It is necessary to wait a long time, sometimes many years, for a large earthquake to occur with similar parameters in approximately the same location.

A second reason is that areas of high seismic activity usually differ widely in geological and seismic characteristics. In addition such areas generally have a high degree of geological inhomogeneity. Both of these factors make the planning of field experiments and the interpretation and comparison of results difficult.

Thirdly, to capture an SEM signal, one must distinguish it from the background, which consists of both natural and man-made EM noise spanning a broad frequency range.

Finally, various research groups have used different measurements and discrimination techniques and frequency ranges, which limits comparison of their results.

Taken together, the above factors have contributed to a lack of consensus among the many research groups which have investigated the existence of SEM phenomena over the past century. Nevertheless we list here some evidence for a positive answer to the question posed in the opening paragraph.

1. The phenomenon of mechano-electromagnetic trans-

Paper number TJE01058.
ISSN: 1681–1208 (online)

The online version of this paper was published December 9, 2001.
URL: http://rjes.agu.org/v03/tje01058/tje01058.htm

duction has been well studied in the laboratory in a wide variety of solids including rocks [*Cress et al.,* 1987; *Kapitsa,* 1955; *Khatiashvili,* 1984; *Nitsan,* 1977; *Ogawa et al.,* 1985; *Parkhomenko,* 1971; *Schloessin,* 1985; *Volarovich and Parkhomenko,* 1955; *Volarovich et al.,* 1962; *Yamada et al.,* 1989].

2. Creation of an electric field by the passage of a seismic wave through soil has been observed [*Eleman,* 1965; *Ivanov,* 1939; *Leland and Rivers,* 1975; *Martner and Sparks,* 1959]. These seismo-electric effects have been applied to geophysical prospecting [*Kepis et al.,* 1995; *Sobolev and Demin,* 1980; *Sobolev et al.,* 1984; *Thompson and Gist,* 1993].

3. The emission of EM signals has been observed in the field experiments over distances as small as tens to hundreds of meters [*Mastov et al.,* 1983, 1984; *Solomatin et al.,* 1983a, 1983b]:

- cave-ins, in large underground cavities which have formed as a result of mining activity;
- before landslides;
- during stress relaxation processes after industrial explosions.

4. The unusual appearance of local atmospheric light seconds or minutes before, and close to the epicenter of, some earthquakes has been witnessed by many individuals [*Derr,* 1973; *Ulomov,* 1971; *Yusui,* 1968]. Obviously, the appearance of atmospheric light implies the existence of strong electric fields.

5. Some pre-seismic data show unusual EM signals. For example, *Fraser-Smith et al.* [1990] monitored EM signals 7 km from the epicenter of the strong Loma Prieta earthquake of 1989. Starting forty days before the quake and continuing for several weeks after the quake, anomalous signals were detected. In particular, three hours before the quake, disturbances began which exceeded the background noise by two orders of magnitude.

The above reasons provide a basis for serious consideration of the existence of SEM phenomena. Such phenomena have been discussed in several monographs and reviews [*Gokhberg et al.,* 1995; *Hayakawa and Fujinawa,* 1994; *Johnston,* 1989, 1997; *Lighthill,* 1996; *Park,* 1996; *Park et al.,* 1993; *Rikitake,* 1976a, 1976b]. We wish to describe briefly a scenario for them based on 1) analysis of experimental field and laboratory data and 2) modeling of electromagnetic emission which incorporates a mechanical model for pre-seismic deformation developed by us over the past fifteen years [*Dobrovolsky et al.,* 1989; *Gershenzon,* 1992; *Gershenzon and Gokhberg,* 1989, 1992, 1993, 1994; *Gershenzon et al.,* 1986, 1987, 1989a, 1989b, 1990, 1993, 1994; *Grigoryev et al.,* 1989; *Wolfe et al.,* 1996]. We have used specific mechanical models of pre-earthquake processes [*Dobrovolsky,* 1991; *Karakin,* 1986; *Karakin and Lobkovsky,* 1985] in some of these articles. But we will not use any of them in this paper because no one model is good enough to describe such complicated processes and developing such a model is not a goal of this paper. Furthermore a specific mechanical model of pre-seismic processes is not needed in constructing a model for SEMS.

The final stage of an earthquake cycle is characterized by stress release processes including foreshocks, the main shock (or swarm), aftershocks, and creep (before and after the earthquake). All of these processes are accompanied by formation of a number of cracks since the Earth's crust consists of extremely brittle materials. So we suppose that the initial source of most SEM anomalies is *a localized high density of cracks.* Such questions as how these localized regions of high crack density are related to the earthquakes, and how far from the earthquake origin and how long before the earthquake they appear, are not considered here. Part of the mechanical energy released in the formation of these cracks is transformed into electromagnetic energy by a variety of mechanisms. Typical "transducer" mechanisms in crustal rocks include piezomagnetic, classical and non-classical piezolectric, electrokinetic and induction. Under appropriate but realistic conditions, phenomena such as quasi-static geomagnetic and electrotelluric anomalies, ultra-low-frequency (ULF) magnetic variations, and radio-frequency (RF) emissions, all associated with preseismic processes, can be explained and estimated on the basis of known mechanical and electromagnetic parameters of the earth's crust.

A comparison of our estimated values of seismo-electromagnetic signals (SEMS) with reported field measurements leads to the conclusion that the sources of most anomalous SEMS are relatively close to the detector. In other words, the source of the signal is *local.* We expect that all pre-earthquake processes, including SEMS, are connected indirectly through global shear stresses, in agreement with Kanamori's interpretation of both SEMS and earthquakes as manifestation of regional geophysical processes [*Kanamori,* 1996].

There is a recognition that clarification of the physical mechanisms of SEMS generation, transmission and reception is needed [*Uyeda,* 1996]. We address these problems in the sections that follow. In section 2 the spectral density of a mechanical disturbance associated with the appearance of a crack is introduced. Section 3 will describe the various coupling mechanisms between a mechanical disturbance and the resulting electromagnetic disturbance. Formulas will be given which relate the parameters of the mechanical disturbance to the parameters which produce the EM disturbance (e.g. magnetization, polarization, current density). This section also includes a comparison of the strengths of these EM sources. Section 4 connects, via Maxwell's equation, the resulting SEMS to the electrical and mechanical parameters of the crust and the characteristics of the mechanical disturbance. The formulas enable us to estimate the spectral density of the SEMS for each type of source considered here. Section 5 describes briefly the morphological features of several observed SEM phenomena, namely tectonomagnetic variation, electrotelluric anomalies, geomagnetic variation in the ultra-low frequency range, and electromagnetic emission in the RF range. The interpretation of these phenomena is discussed based on our model. The paper concludes with a summary of our results and suggestions for future field experiments.

2. Mechanical Model

It is natural to suppose that the origin of SEM anomalies lies in mechanical processes occurring in the earth's crust before an earthquake. The large build-up of mechanical energy during deformation is expended mainly through stress relaxation before, during and after the quake, but a small part goes into EM emission. Note that an important circumstance is that the vibrational spectrum associated with the release of mechanical energy, since it arises, on an atomic scale, from the motion of atoms carrying an electrical charge or a magnetic moment, is related to the spectrum of the EM emission. So if we observe an SEM anomaly of a certain frequency, there must be an associated mechanical disturbance of the same frequency. This does not imply that the corresponding spectral densities are identical, because the electro-mechanical coupling is frequency-dependent. But we would not expect a large EM emission peak in a frequency range where the vibrational spectral density is very small.

A. The Spectral Density of Mechanical Vibrations

Let us consider in more detail the mechanical disturbance associated with the appearance of a crack. Figure 1a shows three different points in the strain field associated with the crack, and Figure 1b shows the variation of strain with time at each of the points.

In this figure, the crack begins to grow at $t = 0$. As it opens, a strain pulse propagates away from the crack, reaching point x_i at time t_i ($i = 1, 2, 3$). The pulse grows to a maximum value and, after it passes, the strain relaxes to a steady value. The maximum and steady values fall off with distance from the crack, but the duration of the pulse, Δt, is constant and given by l_c/V_c where l_c is the crack size and V_c is the crack opening speed (speed of propagation of the crack tip). The quantity V_c is a complicated function of the type of crack, the elastic modulus of the material and the details of the crack formation process, but is less than the velocity of Rayleigh wave [*Kostrov,* 1975] and independent of crack size, having a characteristic value of order 1 km/sec [*Kuksenko et al.,* 1982].

From Figure 1b, we see that the appearance of a crack gives rise to a seismic impulse. The magnitude of this strain impulse is large near the crack and there remains a residual value at long times. We want to estimate the spectral density of mechanical vibrations associated with this impulse. Assume that the change in strain varies with time according to

$$\begin{aligned} &\varepsilon(t,r) = \\ &= \varepsilon_c \exp\left[-\left(\frac{t}{\Delta t}\right)^2\right]\Big[H(r) - H(r-l_c)\Big] + \\ &+ \varepsilon_{\rm imp}(r)\cdot\exp\left[-\left(\frac{t-r/V}{\Delta t}\right)^2\right]H(r-l_c) + \\ &+ \varepsilon_{\rm res}(r)H(t-\Delta t - r/V)\ , \end{aligned} \tag{1}$$

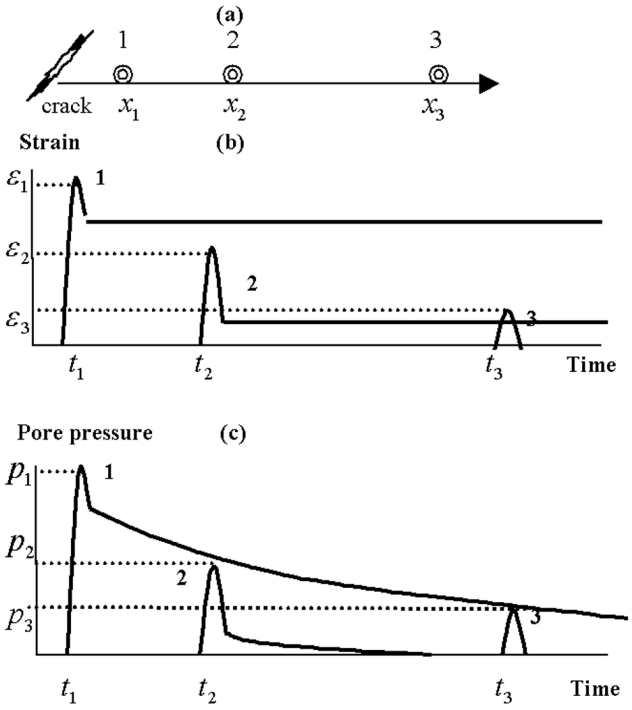

Figure 1. (a) Three different points along the stress field of a crack appearing at t=0. Qualitative sketch of time dependence of strain (b) and pore water pressure (c) at each of these points. The stress field reaches these points at times t_1, t_2, and t_3, with $t_3 > t_2 > t_1 > 0$.

where $H(r)$ is the unit step function ($H(r)$ is zero for $r < 0$ and one for $r > 0$), r is the distance from the crack, V is the elastic wave velocity, ε_c is the average strain change in the vicinity of the crack, $\varepsilon_{\rm imp}(r)$ is the strain change due to the seismic impulse, and $\varepsilon_{\rm res}(r)$ is the change in residual strain due to formation of the crack.

The quantity $\varepsilon_{\rm imp}(r)$ decreases with r as r^{-1} as the pulse propagates away from the crack. But it also is attenuated by the factor $\exp[-r/L]$ due to inelastic processes, where L is the attenuation length. We represent $\varepsilon_{\rm imp}(r)$ as

$$\varepsilon_{\rm imp}(r) \approx \varepsilon_c \cdot \frac{l_c}{r} \cdot \exp\left[-\frac{r}{L}\right]\ . \tag{1a}$$

The attenuation length is a complicated function of frequency, rock structure, temperature and pressure, and can range from 10 to 10,000 wavelengths [*Carmichael,* 1989]. In this paper we shall assume that L lies in the range $10l_c$ to $10^3 l_c$. The strain $\varepsilon_{\rm res}(r)$ falls off with distance much more quickly than $\varepsilon_{\rm imp}(r)$. We assume

$$\varepsilon_{\rm res}(r) \approx \varepsilon_c \cdot \frac{l_c}{r} \cdot \exp\left[-\frac{r}{3l_c}\right] \tag{1b}$$

which expresses the fact that the residual strain extends to about three time the crack size.

Now we can find the spectral density for $\varepsilon(t,r)$ using Equations 1, 1a, and 1b. The result is

$$\varepsilon(\omega,r)=\int_{-\infty}^{\infty}\varepsilon(t,r)\cdot\exp[-i\omega t]\cdot dt=$$
$$=\pi^{1/2}\cdot\varepsilon_c\cdot\Delta t\cdot\exp\left[-\left(\frac{\omega\Delta t}{2}\right)^2\right]\{1+$$
$$+\frac{l_c}{r}\cdot\exp\left[-\frac{r}{L}-i\omega\frac{r}{V}\right]\cdot H(r-l_v)\Big\}+$$
$$+\varepsilon_c\cdot\exp\left[-\frac{r}{3l_c}\right]\cdot\delta(\omega)\ . \tag{1c}$$

The spectrum includes a zero-frequency spike (last term on the right) and a broad, flat spectrum from $\omega = 0$ up to the frequency $\omega_c = (\Delta t)^{-1}$. As we will see in Section 4, the existence of a characteristic pulse lifetime $\tau = L/V$ adds a narrow, flat portion from $\omega = 0$ up to $\omega_{\rm imp} = (\tau)^{-1}$. For $L = 10^2 l_c, V = 3V_c$, and $l_c = 1$ mm, 10^{-1} m and 10 m, the value of ω_c is of order $10^6, 10^4$, and 10^2 rad/s, respectively, and that of $\omega_{\rm imp}$ is $3\cdot10^4$, 300 and 3 rad/s. A result analogous to the preceding expression is obtained for the change in volume strain, $\theta(\omega, r)$.

B. Cracks and the Diffusion of Pore Water

Under natural conditions, practically all rocks contain pore water. In Section 5 we will show that the diffusion of pore water plays a major role in some SEM phenomena.

As shown in Equations A6 and A9 of Appendix A, when monochromatic elastic waves propagate through the crust, the pressure change P is proportional to the volume strain θ for both high and low frequencies. Thus there is a linear coupling between pore pressure and volume fluctuations during a seismic disturbance. This provides us with a means of estimating the relative contribution of pore water diffusion to SEM signals. In particular it enables us to connect changes in crustal deformation and pore water pressure.

Equations A6 and A9 are strictly true only for a monochromatic disturbance. Let's consider again the stress pulse associated with a crack (Figure 1b). While the pulse is growing, the relation between each elastic wave component and the corresponding pore pressure wave component will be given by Equation A6 for high frequencies and Equation A9 for low frequencies. After the pulse passes, leaving a constant residual stress, the pore pressure will relax according to the diffusion Equation A7, as in Figure 1c.

In this figure, the pore pressure has a characteristic diffusion relaxation time ΔT_D (see Equation A7) given by

$$\Delta T_D=\frac{l^2}{D_0}\ , \tag{2}$$

where l is the linear extent of the region in the vicinity of the crack which has appreciable residual stress ($l \approx 3l_c$), and $D_0 = K_2 k_0/\mu_v\beta'$ is the diffusion coefficient. The quantities appearing in D_0 are defined in Appendix A. To estimate the frequency spectrum associated with the pressure change $P(t, r)$ we use an expression similar to Equation 1:

$$P(t,r)=$$
$$=P_0\left\{\exp\left[-\left(\frac{t}{\Delta t}\right)^2\right]\left[H(r)-H(r-l_c)\right]+\right.$$
$$+\frac{l_c}{r}H(r-l_c)\exp\left[-\frac{r}{l_c}-\left(\frac{t-r/V}{\Delta t}\right)^2\right]+$$
$$\left.+\exp\left[-\frac{r}{3l_c}-\left(\frac{t-\Delta t}{\Delta T_D}\right)^2\right]H(t-\Delta t)\right\}\ , \tag{3}$$

where P_0 is the pore water pressure change due to a change of volume strain. We obtain

$$P(\omega,r)=\pi^{1/2}P_0\left\{\Delta t\exp\left[-\left(\frac{\omega\Delta t}{2}\right)^2\right]\left[1+\right.\right.$$
$$\left.+\frac{l_c}{r}H(r-l_c)\exp\left[-(i\omega r/V)\right]\right]+$$
$$\left.+\frac{\Delta T_D}{2}\exp\left[-\frac{r}{3l_c}-\left(\frac{\omega\Delta T_D}{2}\right)^2-i\omega r/V\right]\right\}\ . \tag{3a}$$

From this result we see that the spectrum consists of three parts, a broad low-intensity region (first term) and two low-frequency regions of much higher intensity, one related to the seismic impulse (second term) and the other to a pore water diffusion process (third term). The ratio of the intensities in the first and third regions is $\Delta t/\Delta T_D$. Recall that Δt is given by l_c/V_c. Together with Equation 2 this gives

$$\frac{\Delta t}{\Delta T_D}=\frac{l_c D_0}{(3l_c)^2 V_c}\ .$$

Usually this ratio is much less than one, which means that the process related to water diffusion will dominate in the low frequency range.

From the last two subsections we arrive at the following conclusions. Cracks are a source of two types of mechanical disturbances, a seismic impulse and, in the presence of water-saturated rock, diffusion of pore water. The frequency spectrum of these mechanical disturbances in general will consist of four parts. First there is a zero-frequency spike arising from the residual strain. This spike could potentially be a source of tectonomagnetic anomalies (see Section 5). Second there is a broad spectral range from zero up to high radio frequencies, related to the crack-opening process. The spectral density is nearly flat in this range. Third there is a much narrow spectral range from zero up to low radio frequencies, associated with the seismic impulse generated by the crack. Fourth, there is a low-frequency contribution arising from the diffusion of pore water. This diffusion is driven by the stress associated with crack formation through Equation A7. The spectral density of this part of the spectrum exceeds by several orders of magnitude the broad flat part.

In our model, the basic source of the SEM anomaly is a mechanical deformation resulting in the formation of a large number of cracks. The volume density of cracks, n, cannot exceed the value $n_{\max}$, which, in agreement with laboratory data [*Zhurkov et al.,* 1977], is related to the typical crack length, l_c, via

$$n_{\max}\approx(3l_c)^{-3}\ . \tag{4}$$

If n reaches the value $n_{\max}$, the laboratory sample disintegrates. This implies that n will not exceed $n_{\max}$ in the earth's crust. (Some early estimates of the magnitude of SEM anomalies did not take this restriction on n into account [*Warwick et al.,* 1982].) We therefore express the crack density by the relation

$$n = \alpha n_{\max} \ , \tag{5}$$

where α is the ratio of the actual to the maximum crack density ($0 < \alpha < 1$).

In general, the growth direction of a microcrack is random. But formation of these cracks is a stress-release mechanism, so we would expect that locally there would be some preferred growth direction. Then the average growth direction in a macro-volume undergoing mechanical deformation would be non-zero. In this case the average volume strain, $\bar{\theta}$, and average shear strain, $\bar{\varepsilon}$, are

$$\begin{aligned} \bar{\theta} &= \alpha\theta \ , \\ \bar{\varepsilon} &= \alpha\varepsilon \ , \end{aligned} \tag{5a}$$

where θ and ε are the typical volume and shear strains near a crack.

Formulas (1, 3, 4, 5, and 5a) will be the basis for calculating the magnitude of the various types of SEM anomaly (see sections 4 and 5).

3. Sources of the Electromagnetic Field

In this section we estimate the contribution of possible sources to the EM field. We start by writing Maxwell's equation (in SI units) for an isotropic medium described by electrical permittivity ε, magnetic permeability μ and electrical conductivity σ:

$$\nabla x\vec{E} + \frac{\partial \vec{B}}{\partial t} = 0 \ , \tag{6a}$$

$$\nabla x\vec{H} - \frac{\partial \vec{D}}{\partial t} = \vec{J} \ , \tag{6b}$$

$$\nabla \cdot \vec{B} = 0 \ , \tag{6c}$$

$$\nabla \cdot \vec{D} = \rho \ , \tag{6d}$$

with constitutive relations

$$\vec{B} = \mu\left(\vec{H} + \vec{M}^0\right) \ , \tag{7a}$$

$$\vec{D} = \varepsilon\left\{\vec{E} + \left[1 - \frac{1}{\varepsilon\mu c^2}\right]\vec{u}x\vec{F}\right\} + \vec{P}^0 \ , \tag{7b}$$

$$\vec{j} = \sigma\left(\vec{E} + \vec{E}^0 + \vec{u}x\vec{F}\right) + \vec{j}^{\,0} \ . \tag{7c}$$

Here c is the speed of light, $\vec{u}$ is the velocity of the medium, $\vec{F}$ is the main geomagnetic field, and $\vec{j}^{\,0}, \vec{E}^0, \vec{P}^0$ and $\vec{M}^0$ are the external current density, electric field, polarization and magnetization, respectively.

In general we can classify possible sources into three groups: active, passive and apparent. Examples of active sources are

- changes in the magnetization $\vec{M}^0$ due to mechanical deformation through the piezomagnetic effect
- changes in the polarization $\vec{P}^0$ due either to the piezolectric effect or to non-classical piezolectric effects such as the Stepanov effect [*Stepanov,* 1933]
- the appearance of external currents $\vec{j}^{\,0}$ through the electrokinetic effect due to changes in pore water pressure
- induced currents $\sigma \cdot \vec{u}x\vec{F}$ arising from motion of the medium in the geomagnetic field $\vec{F}$
- an apparent external charge density arising, for example, from charge separation accompanying the formation of a microcrack [*Deryagin et al.,* 1973; *Finkel et al.,* 1985; *Gershenzon et al.,* 1986 *Kornfeld,* 1975]
- the appearance of an external electric field $\vec{E}^0$ due to electrochemical reactions

By passive sources we mean changes in the electromagnetic parameters σ, μ and ε of the earth's crust due to mechanical processes. An example of a passive source is a change in σ in the presence of an external electric field. Such external fields nearly always exist due to magnetospheric/ionospheric geomagnetic variation. Estimation of the effect of passive sources indicates that it is generally much smaller than that of active sources. Therefore we will not consider such sources here, although under special circumstances (e.g. the geometry of local conductivity changes) they may produce anomalies of substantial magnitude [*Honkura and Kubo,* 1986; *Merzer and Klemperer,* 1997; *Rikitake,* 1976a, 1976b].

An example of an apparent source would be the apparent electrotelluric field arising from a change, for whatever reason, of the chemical composition of pore water during measurement of the field, since such a measurement is done using electrodes placed just below the surface [*Miyakoshi,* 1986]. Another example is a change in the apparent local orientation of a detector due to local displacement of the crust. This would give rise to an apparent change in the EM field in the radio frequency range. Sometimes the amount of local displacement needed to give an observed effect is very small. The existence of apparent sources depends on the type of detector and how it is installed, so it is difficult to discuss them in general. However one should keep their existence in mind when interpreting electromagnetic anomalies.

We want to compare the contribution of different active sources. For ease of calculation we assume that the crust is homogeneous and static, i.e. σ, ε and μ are constants independent of location and time. This makes the use of Equations 6 (a–d) and 7 (a–c) convenient. We can eliminate $\vec{H}, \vec{B}$ and $\vec{D}$ and obtain a single equation for the electric field $\vec{E}$ in terms of its sources:

$$\frac{1}{\mu}\nabla x\nabla x\vec{E} + \frac{\sigma\partial\vec{E}}{\partial t} + \varepsilon\frac{\partial^2\vec{E}}{\partial t^2} = \\ = -\left[\frac{\partial}{\partial t}\left(\nabla x\vec{M}^0\right) + \sigma\frac{\partial^2 E^0}{\partial t^2} + \frac{\partial^2\vec{P}^0}{\partial t^2} + \frac{\partial\vec{j}^{\,0}}{\partial t} + \right. \quad (8) \\ \left. + \sigma\frac{\partial\vec{u}}{\partial t}x\vec{F} + \left(1 - \frac{1}{c^2\mu\varepsilon}\right)\frac{\partial^2}{\partial t^2}\left(\vec{u}x\vec{F}\right)\right] .$$

The right-hand side of this equation contains the sources. $\vec{M}^0, \vec{P}^0, \vec{j}^{\,0}, \vec{E}^0$ and $\vec{u}$, which are connected to the mechanical state of the crust through various mechano-electromagnetic coupling mechanisms. In order to estimate and compare the effects of the various sources, we need to write down what these coupling mechanisms are.

A. Piezomagnetic Effect

Some minerals in the earth's crust show residual magnetism due to ferromagnetic inclusions (e.g. titano-magnetite). This residual magnetism was "frozen in" at the time of formation by the paleogeomagnetic field. The deformation of this type of rock leads to changes in $\vec{M}^0$ due to changes in the orientation of the inclusions [*Kapitsa,* 1955; *Kern,* 1961; *Stacey,* 1964; *Stacey and Johnston,* 1972]. These changes are in general a complicated function of the applied stress, the size of the inclusions and the microstructure of the rock, but the following expression is widely used in calculations [*Hao et al.,* 1982; *Zlotnicki and Cornet,* 1986]:

$$M_i^0 = \chi_{||}\left(-{}^3/_2\nabla\sigma_{ij} + 1/2(\nabla\sigma_{kk})\delta_{ij}\right) I_j \ , \quad (9)$$

where $\chi_{||}$ is the stress sensitivity in the direction parallel to the axial load, σ_{ij} is the stress tensor, $\vec{I}$ is the reference magnetization and repeated indexes are summed. In terms of the strain tensor ε_{ij} and the shear modulus μ_s, we can write

$$M_i^0 = \mu_s\chi_{||}\left(\varepsilon_{ij} - 2\varepsilon_{kk}\delta_{ij}\right) I_j \ . \quad (10)$$

B. Piezoelectric Effect

One of the most commonly occurring minerals, quartz, shows this effect, namely, the occurrence of an electric polarization under the influence of mechanical stress [*Parkhomenko,* 1971; *Volarovich and Parkhomenko,* 1955]. Usually, quartz grains are randomly oriented and show very weak piezolectricity in the aggregate. But because of residual orientation of the quartz grains some rocks will show a larger piezolectric effect [*Ghomshei and Templeton,* 1989], although still perhaps two to three orders of magnitude less than in monocrystalline quartz [*Bishop,* 1981]. The piezolectric properties of rocks have been widely studied in the context of geophysical prospecting [*Kepis et al.,* 1995; *Neyshtadt et al.,* 1972; *Sobolev and Demin,* 1980; *Sobolev et al.,* 1984]. Changes in polarization can be related to the strain tensor via

$$P_k^0 = D_{kij}\mu_s\left(\varepsilon_{kk}\delta_{ij} + 2\varepsilon_{ij}\right) \ , \quad (11)$$

where D_{kij} is the piezolectric modulus. For making estimates, we consider only the contribution from $i = j = 1$. The magnitude of D_{kij} depends on the scale of the mechanical disturbance. If this scale is of the order of the diameter of a typical quartz grain ($\sim$0.5 mm) then $D \equiv D_{k11} \approx -2.3 \times 10^{-12} C/N$; if the scale is much larger than this we will take $D \approx -10^{-14} C/N$ [*Bishop,* 1981].

It is possible for the polarization to change for reasons other than the classical piezolectric effect. All real crystals contain extended defects (dislocations). In dielectric materials, dislocations usually are charged because point defects are associated with them. Under static conditions the charge around the dislocation is neutralized by point defects of opposite charge (the Debye-Huckel cloud). Under the influence of an applied stress the dislocation can move. At nearly all temperatures of interest an unpinned dislocation will move much more quickly than its associated Debye-Huckel cloud and therefore will carry a net charge along with it. This will give rise to charge transport and polarization of the material. This effect was discovered by Stepanov [*Stepanov,* 1933]. Its magnitude is a complicated function of dislocation density, density and type of point defects, temperature and pressure. Because rocks have an extremely high density of dislocations and point defects, pinning effects will make dislocation movement almost impossible at normal temperatures in these materials; at greater depths where the temperature and pressure are greater this effect could be important [*Slifkin,* 1996]. There are some mechanisms related to movement or polarization of point defects which also lead to the appearance of an electric field. One of these effect is the so called "pressure stimulated current" [*Varotsos and Alexopoulos,* 1986]. Another mechanism for polarization of the crust is directly associated with crack formation [*Cress et al.,* 1987; *Khatiashvili,* 1984; *Nitsan,* 1977; *Ogawa et al.,* 1985; *Schloessin,* 1985; *Warwick et al.,* 1982; *Yamada et al.,* 1989]. It is well known that the appearance of a crack in almost any material produces effects such as light bursts, electron streams and broad-band electromagnetic emission up to x-ray frequencies [*Deryagin et al.,* 1973; *Finkel et al.,* 1985; *Gershenzon et al.,* 1986]. These phenomena are due to the electric field (up to 10^8 V/m) associated with a buildup of high electric charge density on the new surfaces of the emerging crack. This effect has been studied by several groups and is another type of non-classical piezolectric effect. It is almost impossible to estimate theoretically the contribution from this mechanism since there are many different effects which accompany crack formation and many unknown parameters, but it could be important in high-frequency SEM phenomena.

C. Electrokinetic Effect

As mentioned above, under natural conditions rocks practically always contain pore water. At the pore boundary there exists an electric double layer due to the difference in the electrochemical potentials of water and rock. Deformation of the earth's crust leads to changes in pore pressure and, as a consequence, diffusion of the pore water in a direction opposite the pressure gradient. The motion of this water layer next to the pore boundary results in charge transport, i.e. an electric current, parallel to the boundary. This phenomenon was discovered in the mid-nineteenth century and was first used in a geophysical context by *Frenkel* [1944] to explain the observations of *Ivanov* [1939]. More recently it has been used in explaining and modeling SEM phenomena [*Ishido and Mizutani,* 1981; *Mizutani and Ishido,* 1976; *Mizutani et al.,* 1976] and in geophysical prospecting [*Maxwell et al.,* 1992; *Sobolev and Demin,* 1980; *Thompson and Gist,* 1993; *Wolfe et al.,* 1996]. The relation between the electrokinetic current density $\vec{j}^0$ and pore pressure P can be written as

$$\vec{j}^0 = \sigma C \nabla P \ , \tag{12}$$

where C is the coefficient of the streaming potential. The pressure is related to the volume strain by Equation A1 (Appendix 1).

D. Induction Effect

Movement of conducting crustal material in the geomagnetic field gives rise to an induced electric field $\vec{u}x\vec{F}$ and current $\vec{j} = \sigma \vec{u}x\vec{F}$. There are two possible sources of this movement; one is the deformation and movement of rock material itself and the other is diffusion of pore water due to volume deformation. In the first case the velocity $\vec{u}$ of the crustal material is related to the strain tensor e_{ij} by

$$u_i = e_{ij} V_j \ , \tag{13}$$

where $\vec{V}$ is the velocity of elastic waves. This formula reflects the fact that any change in strain is propagated through the crust at the seismic velocity.

In the case of induction due to pore water movement the effective velocity $\vec{u}$ can be estimated by Darcy's law,

$$\vec{u} = k_0 \nabla P / m\mu_v \ , \tag{14}$$

where P is given in Equation A9 and the parameters k_0, m and μ_v are defined in Appendix A.

Now that we have expressed all the terms on the right-hand side of Equation 8 in terms of electromechanical coefficients and strain changes, we can compare different kinds of sources. Let's consider the terms

$$A_m = \left| \nabla x \vec{M}^0 \right| \ , \tag{15a}$$

$$A_p = \left| \frac{\partial \vec{P}^0}{\partial t} \right| \ , \tag{15b}$$

$$A_j = \left| \vec{j}^{\,0} \right| \ , \tag{15c}$$

$$A_I = \left| \vec{u}x\vec{F} + \left(1 - \frac{1}{c^2 \mu\varepsilon}\right) \frac{d}{dt}(\vec{u}x\vec{F}) \right| \ , \tag{15d}$$

which are piezomagnetic, piezolectric, electrokinetic and induction sources, respectively. We have two types of induction sources, a source A_{I1} due to deformation and movement of rock material itself and a source A_{I2} due to diffusion of pore water. It is easy to show that the second term in relation 15d is small compared with the first term, and we shall neglect it. Replacing $\frac{\partial}{\partial t}$ with $\frac{V_c}{l_c}$ and $\frac{\partial}{\partial r}$ with $\frac{1}{l_c}$, we can find the ratios of the strengths of the various transducer mechanisms using Equations 9 through 14 and A9:

$$\frac{A_m}{A_p} = \frac{I\chi_{||}}{V_c D} \ , \quad \frac{A_m}{A_j} = \frac{2\mu_s \chi_{||} I \beta'}{\sigma C K_2 \beta} \ ,$$

$$\frac{A_m}{A_{I1}} = \frac{2\chi_{||}\mu_s I}{\sigma V F l_c} \ , \quad \frac{A_j}{A_{I2}} = \frac{Cm\mu_s}{Fk_0} \ .$$

Table 1a shows the results of comparing these strengths for the values of D, C, l_c and k_0 given in Table 1b. The values of the remaining coefficients appearing in these ratios may be obtained from Table 6 (see Appendix A). We see that the strength of a piezomagnetic source has the same order of magnitude as that of piezolectric pure quartz. Monocrystalline quartz occurs in nature only as small grains (<1 mm), which have practically no preferred orientation ($D = D_1$). For such small grains a piezolectric source would be important only in the radio-frequency range. If the piezolectric grains were to have a preferred orientation on a macro-scale ($D = D_2$), we would expect their source strength to be at least two orders of magnitude weaker than a piezomagnetic one.

Referring again to Table 1a, comparison of piezomagnetic and electrokinetic sources shows that under some conditions, namely high (but still reasonable) values of electrical conductivity σ and electro-streaming potential C, an electrokinetic source could have a strength of the same order of magnitude as a piezomagnetic or piezolectric source. For low conductivity ($\sigma < 10^{-3}/\Omega - m$) the piezomagnetic source exceeds the electrokinetic source.

The three types of sources considered above have the same dependence on the source size; for this reason the latter does not enter into the comparison of their relative strengths. In the case of an induction source of type 1 (A_{I1}), the induction source strength relative to the strength of any of the other three sources depends on the size of the source. We can see from Table 1a (first column/fourth row) that the piezomagnetic source essentially exceeds the induction source A_{I1} on small to medium size scales; the induction source A_{I1} becomes important only for a source size greater than 1 km and high electrical conductivity ($\sigma > 10^{-1}/\Omega - m$).

Table 1. Comparison of the strengths of various mechano-electromagnetic transducers. Each entry gives the (column header)/(row header) strength ratio for the parameter values of D, C, l_c and k_0 given in Table 1a

		A_m	A_p		A_j		A_{I1}			A_{I2}	
			D_1	D_2	C_1	C_2	l_{c1}	l_{c2}	l_{c3}	k_{01}	k_{02}
A_m			2.3	10^{-2}	1.5	0.15	$4\cdot10^{-7}$	$4\cdot10^{-4}$	0.4	$1.5\cdot10^{-5}$	$1.5\cdot10^{-9}$
A_p	D_1	0.4			0.7	$7\cdot10^{-2}$	$2\cdot10^{-7}$	$2\cdot10^{-4}$	0.2	$6\cdot10^{-6}$	$6\cdot10^{-10}$
	D_2	10^2			150	15	$4\cdot10^{-5}$	$4\cdot10^{-2}$	40	1.5	$1.5\cdot10^{-7}$
A_j	C_1	0.7	1.5	$0.7\cdot10^{-2}$			$3\cdot10^{-7}$	$3\cdot10^{-4}$	0.3	10^{-5}	10^{-9}
	C_2	7	15	$0.7\cdot10^{-1}$			$3\cdot10^{-6}$	$3\cdot10^{-3}$	3	10^{-4}	10^{-8}
A_{I1}	l_{c1}	$2.4\cdot10^6$	$6\cdot10^6$	$2.4\cdot10^4$	$3.6\cdot10^6$	$3.6\cdot10^5$				36	$3.6\cdot10^{-3}$
	l_{c2}	$2.4\cdot10^3$	$6\cdot10^3$	$2.4\cdot10$	$3.6\cdot10^3$	$3.6\cdot10^2$				$3.6\cdot10^{-2}$	$3.6\cdot10^{-6}$
	l_{c3}	2.4	6	$2.4\cdot10^{-2}$	3.6	0.36				$3.6\cdot10^{-5}$	$3.6\cdot10^{-9}$
A_{I2}	k_{01}	$7\cdot10^6$	$1.5\cdot10^5$	$7\cdot10^2$	10^5	10^4	$3\cdot10^{-2}$	30	$3\cdot10^4$		
	k_{02}	$7\cdot10^8$	$1.5\cdot10^9$	$7\cdot10^6$	10^9	10^8	$3\cdot10^2$	$3\cdot10^5$	$3\cdot10^8$		

Both electrokinetic sources and induction sources of the second type (A_{I2}) arise from diffusion of pore water, so they occur together. We see that the induction source A_{I2} is always much less than the electrokinetic source. Even if the water layer in the crust has an extremely high permissibility ($k_0 \approx 10^{-10}$ m^2) the electrokinetic source exceeds A_{I2} by two to three orders of magnitude. For usual values of permissibility ($k_0 = 10^{-12}$ to 10^{-16} m^2), the difference in source strength ranges from four to nine orders of magnitude.

The preceding considerations lead us to the following conclusions. For small sources, the most important mechano-electromagnetic processes considered here are the piezomagnetic, electrokinetic and piezolectric. For large sources, only piezomagnetic and electrokinetic processes are important. The induction effect is important only on a very large size scale, when the source size is comparable to the earthquake focal zone.

4. The Electromagnetic Field of an Impulse Dipole

Comparison of the strengths of the various types of sources using scaling arguments as in Section 3 gives us some superficial information about relative strengths. More accurate results would require solving the system of Equations 6(a–d), 7(a–c), and the appropriate equation connecting the magnetization or polarization to the mechanical state of the crust (cf. Equations 9–14). In general such solutions cannot be obtained analytically without some simplification.

Table 1a. Parameter values used in Table 1

D_1	-2.3×10^{-12} C/N	k_{01}	10^{-12} m^2
D_2	-10^{-14} C/N	k_{02}	10^{-16} m^2
C_1	10^{-6} V/Pa	σ	$10^{-1}/\Omega - m$
C_2	10^{-7} V/Pa	I	1.5 A/m
l_{c1}	10^{-3} m	$\chi_{\|\|}$	-2×10^{-9} Pa^{-1}
l_{c2}	1 m	F	3×10^{-5} T
l_{c3}	10^3 m	$V(=3V_c)$	3×10^3 m/s

The goal of this section is to present a set of asymptotic formulas for estimating the magnitude of the electric and magnetic fields at the earth's surface over a broad frequency range, ranging from quasi-static to radio frequencies, generated by mechanical disturbances in the earth's crust. We will also present the results of calculations of the spectral density of an EM source produced by an impulse mechanical source due to various mechano-electromagnetic coupling mechanisms.

First we consider the electromagnetic fields to be weak enough that they do not influence the mechanical state, i.e. the stress and strain tensors are independent of $\vec{E}$ and $\vec{H}$. We also assume that the size of the source is much smaller than the distance from the source to the field point (dipole approximation). We are ignoring higher-order multipoles; their effect is normally negligible unless the dipole moments vanish. Introducing a distribution of effective electric and magnetic dipoles characterized by $\vec{P}^*$ and $\vec{M}^*$, respectively, the system of Equations 6(a–d) can be written as follows [*Gershenzon et al.,* 1993]:

$$\nabla x\vec{E} + \frac{\partial}{\partial t}\left[\mu\vec{H} + \vec{M}^*\delta(\vec{r})\right] = 0\ , \tag{16a}$$

$$\nabla x\vec{H} - \frac{\partial}{\partial t}\left(\varepsilon\vec{E}\right) - \sigma\vec{E} = \vec{P}^*\delta((\vec{r})\ , \tag{16b}$$

$$\nabla\cdot\vec{H} = -\vec{M}^*\cdot\nabla\delta(\vec{r})\ , \tag{16c}$$

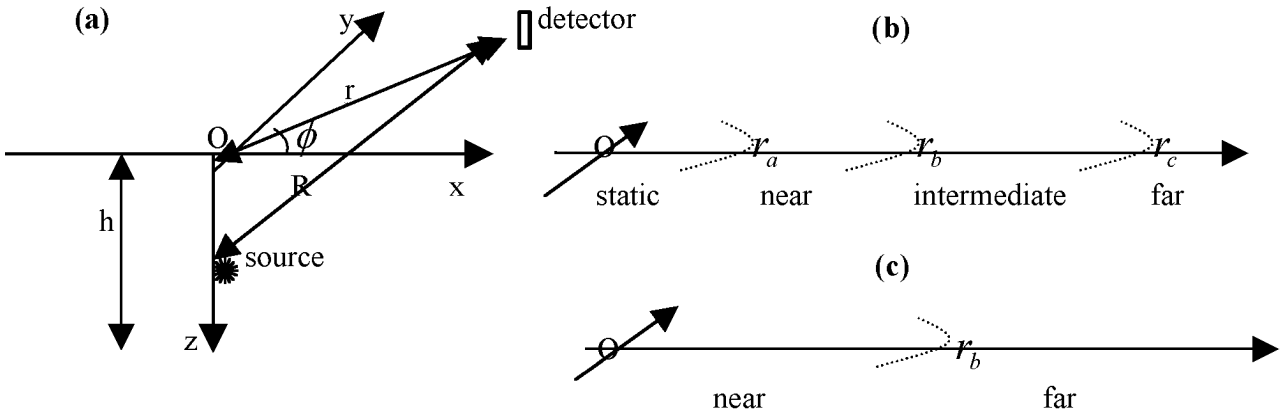

Figure 2. (a) Coordinate system, showing a detector on the surface (taken as the xy plane) and a source located on the z-axis at depth h below the surface. (b) The four asymptotic regions for $\sigma/\omega\varepsilon > 1$. (c) The two asymptotic regions for $\sigma/\omega\varepsilon < 1$.

$$\nabla \cdot \left[\frac{\partial}{\partial t} \left(\varepsilon \vec{E} \right) + \sigma \vec{E} \right] = \vec{P}^* \cdot \nabla \delta \left(\vec{r} \right) \ , \tag{16d}$$

where

$$\vec{P}^* = \overline{J}^0 + \frac{\partial \overline{P}^0}{\partial t} \ , \tag{17a}$$

$$\vec{M}^* = \overline{M}^0 + \frac{1}{2} \int\limits_{\infty} \vec{r} x \vec{J}^0_{\text{rot}} dV \ , \tag{17b}$$

and the bar symbol indicates an integration over volume, i.e., $\overline{J}^{\,0} \equiv \int\limits_{\infty} \vec{J}^0 dV$, etc. We also have

$$\begin{aligned} \vec{J}^0 &= \sigma \left(\vec{E}^0 + \vec{u} x \vec{F} \right) + \vec{j}^{\,0} + \\ &+ \varepsilon \left[1 - \frac{1}{c^2 \varepsilon \mu} \right] \frac{\partial}{\partial t} \left(\vec{u} x \vec{F} \right) \ , \end{aligned} \tag{17c}$$

and

$$\vec{J}^0 = \vec{J}^0_{\text{rot}} + \vec{J}^0_{\text{irrot}} \ . \tag{17d}$$

As expressed in Equation 17d, we can always consider $\vec{J}^0$ as the sum of two contributions, a rotational part $\vec{J}^0_{\text{rot}}$ associated with magnetic dipoles and an irrotational part $\vec{J}^0_{\text{irrot}}$ associated with electric dipoles.

We consider our source to be embedded at depth h in a homogenous static conducting half-space (the crust) with conductivity σ, dielectric constant ε and magnetic susceptibility μ. We want to find the EM fields near the air-crust interface as a function of the azimuthal angle ϕ and the distance r from the coordinate origin O (see Figure 2a).

A. Asymptotic Formulas for $r > \left| \left(\omega^2 \mu\varepsilon + i\omega\mu\sigma \right)^{-1} \right|$ and $\omega < \sigma/\varepsilon$

The next simplification is to consider a monochromatic source. The radiation due to a monochromatic point dipole in a conducting half-space is a classical problem first considered by Sommerfeld. The full results may be found in the monograph by *Banos* [1966] and we shall use them here. For points near the interface the solution has a particularly simple asymptotic form. The specific form of the solution depends on whether the field point is in the so-called near zone, intermediate zone, or far zone. These zones are characterized by distance from the hypocenter, frequency and the electromagnetic parameters of the medium. In terms of the distance parameters r_A, r_B and r_C, we have $r_A \ll r \ll r_B$ in the near zone, $r_B \ll r \ll r_C$ in the intermediate zone and $r \gg r_C$ in the far zone. The distances r_A, r_B, and r_C are defined by

$$|k_1 r_A| = 1, \ |k_2 r_B| = 1, \ \left| n^2 k_2 r_C \right| = 1,$$

$$k_1^2 = \omega^2 \mu\varepsilon + i\omega\mu\sigma, \ k_2^2 = \omega^2 \mu_0 \varepsilon_0, \ n = k_2/k_1 \ .$$

We shall estimate the value of these distances for typical values of σ, ε and μ. In this paper we shall take $\varepsilon = 3\varepsilon_0$ and $\mu = \mu_0$ for the crust, where ε_0 and μ_0 are the values in vacuum. Most frequencies $f = \omega/2\pi$ of interest lie in the range 10^{-3} Hz $< f < 10^7$ Hz and the conductivity of most rocks is in the range $10^{-5} \leq \sigma \leq 10^{-1}/\Omega - m$. Figure 3 shows the dependence of r_A, r_B and r_C on frequency for three different values of σ. We are interested in distance less than 1000 km. From the figure we see that the Banos formulas cannot be used in the quasi-static regime ($f < 10^{-2}$ Hz) except for large conductivities ($\sigma > 10^{-1}/\Omega - m$.) and for distances $r > 10$ km, since r must be greater than r_A and here $r_A = 10$ km for $\sigma = 10^{-1}/\Omega - m$ and $f = 10^{-2}$ Hz.

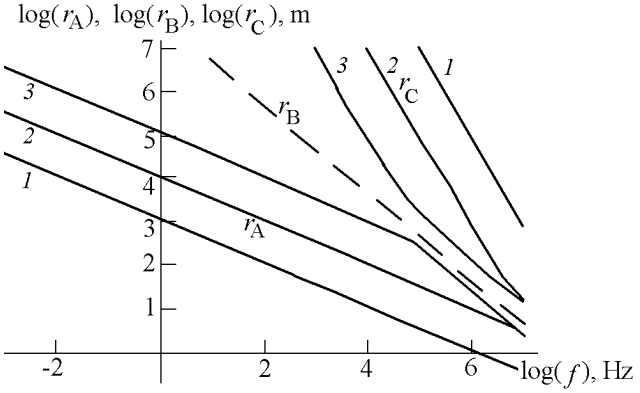

Figure 3. The frequency dependence of the distances r_A, r_B and r_C in Figure 2, for various values of conductivity. (1) $\sigma = 10^{-1}/\Omega - m$; (2) $\sigma = 10^{-3}/\Omega - m$; (3) $\sigma = 10^{-5}/\Omega - m$. The distance r_B (dashed line) is independent of σ.

In the ultra-low frequency (ULF) range (10^{-2} Hz $< f <$ 10 Hz) the near zone approximation has a broader range of applicability. For RF frequencies up to 10^4 Hz, either the near zone or intermediate zone formulas will apply. For RF frequencies greater than 10^4 Hz the near, intermediate and far zone formulas can be used for almost all cases except for low conductivities and high frequencies, i.e. when $\omega > \sigma/\varepsilon$. Then $r_A \approx r_B \approx r_C$, the displacement current in the crust approaches the conductive current, and the Banos formulas no longer apply.

The expressions for the fields close to the surface for monochromatic electric and magnetic dipoles [*Banos,* 1966] are given in Appendix B. At the interface, all these expressions will contain the complex exponential factor $e^{ik_1 h}$, which includes the attenuating effect of the crust. Introducing the parameter

$$\omega_h = \left(\frac{2}{h^2 \mu \sigma}\right)^{1/2} ,$$

the exponential can be written,

$$e^{ik_1 h} = e^{i(\omega/\omega_h)^{1/2}} \cdot e^{-(\omega/\omega_h)^{1/2}} .$$

For $\omega \gg \omega_h$ the attenuation will make the fields negligible at the interface. For $\omega \ll \omega_h$ there is no appreciable attenuation and the radiation propagates along the surface away from the hypocenter as an inverse power of the distance.

B. Asymptotic Formulas for $r < \left|\left(\omega^2 \mu\varepsilon + i\omega\mu\sigma\right)^{-1}\right|$

For distances $r > r_A$, the formulas of *Banos* [1966] could be used. However, as we have seen, in the quasi-static range and part of the ULF range, these formulas do not apply because r_A exceeds the range of interest. Even at higher frequencies, when r_A becomes small, we need a formula for $r < r_A$. In this situation we estimate the fields using the static or zero-frequency limit. This will be valid for frequencies whose associated skin-depth δ is much greater than h: $\delta = (2/\omega\mu\sigma)^{1/2} \gg h$. In this zero-frequency approximation, any electric field produced by the magnetic dipole is ignored.

For a static magnetic dipole, we have $\vec{E} = 0$ and

$$\vec{B} = \frac{\mu}{4\pi} \frac{3\hat{R}\left(\vec{M}^* \cdot \hat{R}\right) - \vec{M}^*}{R^3} , \tag{18a}$$

where R is the distance from the source.

For a static electric dipole embedded in a conducting halfspace, we use

$$\begin{aligned} \vec{E}_x &= \frac{P^*}{2\pi\sigma} \frac{1}{R^3} \left(\frac{3x^2}{R^2} - 1\right), \\ E_y &= \frac{P^*}{2\pi\sigma} \frac{3xy}{R^5}, \quad E_z = 0 , \end{aligned} \tag{18b}$$

$$\begin{aligned} B_x &= \frac{\mu P^*}{4\pi} \frac{xy}{r^4 R^3} \left[2R^3 - h(2h^2 + 3r^2)\right] , \\ B_y &= \frac{\mu P^*}{4\pi} \frac{(x^2 - y^2)(R^3 - h^3) + 3hy^2 z^2}{r^4 R^3} , \\ B_z &= \mu P^* \frac{y}{R^3} , \end{aligned} \tag{18c}$$

if the dipole is oriented horizontally along the x axis, and

$$\begin{aligned} E_x = -\frac{P^*}{2\pi\sigma} \frac{3hy}{R^5}, \; E_y = -\frac{P^*}{2\pi\sigma} \frac{3hx}{R^5}, \\ E_x = 0, \; B = 0 , \end{aligned} \tag{18d}$$

if the dipole is vertical. These formulas were obtained in the point dipole limit of expressions given by *Edwards* [1975] and *Gokhberg et al.* [1985].

C. Asymptotic Formulas for $\omega > \sigma/\varepsilon$

Now consider the case $\omega > \sigma/\varepsilon$, for which the Banos formulas do not apply. For this case we can ignore the conductivity of the crust (as long as the source depth is less than the skin depth) and use formulas appropriate to a dipole in vacuum. For distance r less than r_B (i.e. less than the vacuum wavelength/2π), the following formulas [*Landau and Lifshitz,* 1971]:

$$\vec{E}(\omega) = \frac{3\hat{R}(\hat{R} \cdot (\vec{P}^*(\omega)/\omega)) - \vec{P}^*(\omega)/\omega}{4\pi\varepsilon R^3} , \tag{19a}$$

$$\vec{B}(\omega) = -\frac{\mu}{4\pi} \frac{\vec{P}^*(\omega) x \hat{R}}{R^2} , \tag{19b}$$

for an electric dipole, and

$$\vec{E}(\omega) = -\frac{\omega \vec{M}^*(\omega) x \hat{R}}{4\pi\varepsilon c^2 R^2} , \tag{19c}$$

$$\vec{B}(\omega) = \frac{\mu}{4\pi}\frac{3\hat{R}(\hat{R}\cdot\vec{M}^*(\omega)) - \vec{M}^*(\omega)}{R^3}\ , \tag{19d}$$

for a magnetic dipole.

For distances r greater than r_B, we have [*Landau and Lifshitz,* 1971]

$$\vec{E}(\omega) = \frac{\omega\left[\left[\vec{P}^*(\omega)x\hat{R}\right]x\hat{R}\right]}{4\pi\varepsilon c^2 R}\ , \tag{20a}$$

$$\vec{B}(\omega) = \frac{\mu}{4\pi c}\frac{\omega\vec{P}^*(\omega)x\hat{R}}{R} \tag{20b}$$

for an electric dipole, and

$$\vec{E}(\omega) = \frac{\omega^2\vec{M}^*(\omega)x\hat{R}}{4\pi\varepsilon c^3 R}\ , \tag{20c}$$

$$\vec{B} = \frac{\mu}{4\pi c^2}\frac{\omega^2\left[\left[\vec{M}^*(\omega)x\hat{R}\right]x\hat{R}\right]}{R} \tag{20d}$$

for a magnetic dipole.

D. Spectral Density of Electric and Magnetic Dipoles

Once we have a solution for the monochromatic source the standard procedure for solving the time-dependent problem is to integrate the monochromatic solution over all frequencies, weighted by the spectral density of the source. In order to estimate the parameters of the EM emission it is useful to consider an impulse dipole source, since the mechanical disturbances have an impulse structure (see Section 2).

Using Equations 17(a–d), 10–14, 1, 1(a–b) and 3, we can express the electric and magnetic dipoles for all the source types considered here. For a piezomagnetic source, the magnetic dipole has the following form:

$$\begin{aligned}\vec{M}^*(t) = \vec{M}_M\Big\{&\exp\left[-\left(\frac{t}{\Delta t}\right)^2\right] + \\ &+\int\limits_V \frac{l_c}{r}H(r-l_c)\exp\left[-\frac{r}{L}-\left(\frac{t-r/V}{\Delta t}\right)^2\right]\frac{dV}{l_c^3}+ \\ &+\int\limits_V H(r-\Delta t-r/V)\exp\left[-\frac{r}{3l_c}\right]\frac{dV}{l_c^3}\Big\}\ ,\end{aligned} \tag{21a}$$

where

$$\vec{M}_M = \int\limits_{V_{\text{crack}}}\vec{M}^0 dV \tag{21a'}$$

and the integral is over the volume $V_{\text{crack}} = l_c^3$ associated with a crack. The magnetic and electric dipoles for an induction source have essentially the same form as Equation 21a, except that the third term is absent and $\vec{M}_I$ and $\vec{P}_I$ appear in place of $\vec{M}_M$. The electric dipole for an electrokinetic source has the form shown in Equation 21b:

$$\begin{aligned}\vec{P}^*(t) = \vec{P}_K\Big\{&\exp\left[-\left(\frac{t}{\Delta t}\right)^2\right] + \\ &+\int\limits_S \frac{l_c}{r}H(r-l_c)\exp\left[-\frac{r}{L}-\left(\frac{t-r/V}{\Delta t}\right)^2\right]\frac{dS}{l_c^2}+ \\ &+\int\limits_S H(r-\Delta t-r/V)\exp\left[-\frac{r}{3l_c}-\left(\frac{t-r/V}{\Delta T_D}\right)^2\right]\frac{dS}{l_c^2}\Big\}\ ,\end{aligned} \tag{21b}$$

where

$$\vec{P}_K = \int\limits_{V_{\text{crack}}}\vec{j}^{\,0}dV\ . \tag{21b'}$$

The electrokinetic source appears as a discontinuity in the electrokinetic properties of the medium across a planar boundary, so the last two terms in Equation 21b are expressed as surface integrals rather than volume integrals. See Appendix C for a more detailed explanation.

For a piezolectric source, the electric dipole can be expressed as

$$\begin{aligned}\vec{P}^*(t) = \frac{d}{dt}\Bigg\{&\vec{P}_E\exp\left[-\left(\frac{t}{\Delta t}\right)^2\right] + \\ &+\left|\vec{P}_E\right|\int\limits_V \hat{n}(\vec{r})\frac{l_c}{r}H(r-l_c)\exp\left[-\frac{r}{L}-\left(\frac{t-r/V}{\Delta t}\right)^2\right]\frac{dV}{l_c^3}\Bigg\}\ ,\end{aligned} \tag{21c}$$

where

$$\vec{P}_E = \int\limits_{V_{\text{crack}}}P^0 dV \tag{21c'}$$

and $\hat{n}(\vec{r})$ is a unit vector in the direction of the local dipole moment in the volume element dV at point $\vec{r}$ in the crust. This local moment has magnitude $\left|\vec{P}_E\right|$ attenuated by the factor $(l_c/r)e^{-r/L}$. The magnitudes of M_M, M_I, P_I, P_K and P_E will be determined later in this section.

Now we can find the associated spectral densities. For a piezomagnetic source we have,

$$\begin{aligned}\vec{M}^*(\omega) &= \int\limits_{-\infty}^{\infty}\vec{M}^*(t)\exp[-i\omega t]dt = \\ &= \vec{M}_M\left\{\pi^{1/2}\Delta t\exp\left[-\left(\frac{\omega\Delta t}{2}\right)^2\right]\times\right. \\ &\left.\times\left[1+\frac{L^2}{l_c^2}\frac{1}{1+(\omega\tau)^2}\right]+27\pi^2\delta(\omega)\right\}\ ,\end{aligned} \tag{22a}$$

where $\tau = L/V$ is the lifetime of the seismic impulse. The same expression (without the last term) also gives the spec-

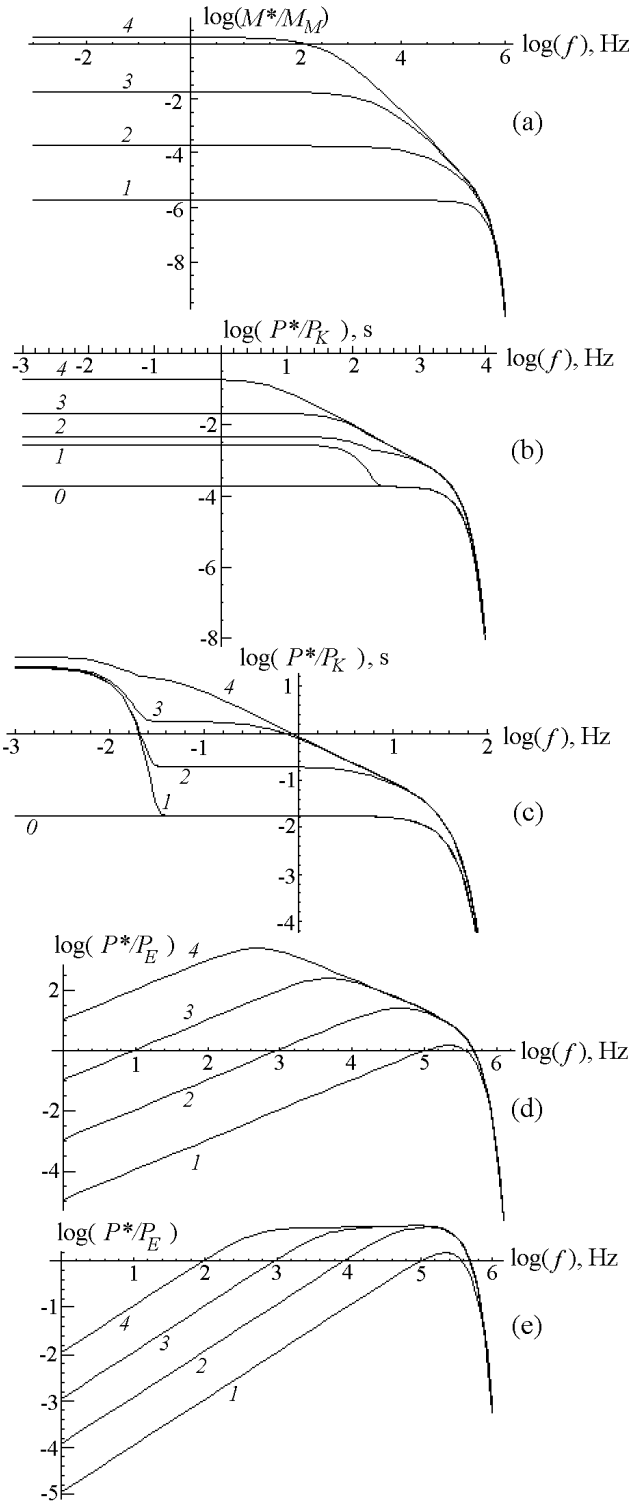

Figure 4. Spectral densities associated with various types of sources. In each graph, curves 1–4 correspond to $L = l_c, 10l_c, 10^2 l_c$ and $10^3 l_c$, respectively. (a) Piezomagnetic source, $l_c = 10^{-3}$ m. (b) Electrokinetic source, $l_c = 0.1$ m, $\mu_v = 10^{-12}\mathrm{m}^2$, curve (0) corresponds to $L = l_c$ with no diffusion term. (c) Electrokinetic source, same as (b) except that $l_c = 10$ m. (d) Piezolectric source, $l_c = 10^{-3}$ m, $V_S = 3 \cdot 10^3$ m/s, partially ordered grains. (e) Piezoelectric source, $l_c = 10^{-3}$ m, $V_S = 3 \cdot 10^3$ m/s, randomly oriented grains.

tral density for the magnetic and electric dipoles of an induction source.

Figure 4a shows $M^*(\omega)$ for various value of L. Curve 1 ($L = l_c = 1$ mm) is the contribution of only the microcrack and corresponds to the first term in Equation 22a. It consists of a zero-frequency spike (not shown in the figure because of the logarithmic scale) and a broad, flat spectrum extending from zero up to $\omega_c = (\Delta t)^{-1}$, with magnitude $M_M \pi^{1/2} \Delta t$. The contribution of the impulse (curves 2–4) increases the spectral density magnitude by the factor $(L/l_c)^2$ and shifts the spectrum to a lower frequency range ($0 < \omega < \omega_{\mathrm{imp}} \equiv \tau^{-1}$).

Using Equation 21b we can find the spectral density associated with an electrokinetic source. We obtain

$$\vec{P}^*(\omega) = \vec{P}_K \pi^{1/2} \left\{ \Delta t \exp\left[-\left(\frac{\omega \Delta t}{2} \right)^2 \right] \times \right.$$
$$\times \left[1 + \frac{L}{l_c} \frac{1}{1 + (\omega\tau)^2)^{1/2}} \right] + \qquad (22b)$$
$$\left. + \frac{\Delta T_D}{2} \exp\left[-\left(\frac{\omega \Delta T_D}{2} \right)^2 \right] \right\} .$$

Figures 4b and 4c show $P^*(\omega)$ for several values of L, including the cases $L = l_c = 0.1$ m (Figure 4b) and $L = l_c = 10$ m (Figure 4c). In both cases, curve 0 represents the contribution of the crack itself and corresponds to the first term in Equation 22b. Including the diffusion of pore water (third term) results in curve 1. Including the contribution of the impulse (second term) results in curves 2–4. The impulse contribution scales as (L/l_c). From these figures we see that the contribution of the diffusion and impulse terms exceeds that of the crack itself at low frequencies. For a small crack (Figure 4b) the impulse contribution exceeds the diffusion contribution, but for a large crack (Figure 4c) the diffusion term dominates.

Finally, we consider the spectral density associated with a piezolectric source. The orientation of piezolectric grains are usually random, but in some cases may be partially ordered. We need to consider both cases. First, suppose there is a preferred orientation $\hat{n} = \vec{P}_E / P_E$. Using Equation 21c we find

$$\vec{P}^*(\omega) = \vec{P}_E \pi^{1/2} \omega \Delta t \exp\left[-\left(\frac{\omega \Delta t}{2} \right)^2 \right] \times$$
$$\times \left[1 + \frac{L^2}{l_c^2} \frac{1}{1 + (\omega\tau)^2} \right] . \qquad (22c)$$

Figure 4d shows this spectral density. As before, curve 1 is for the crack only. The presence of the seismic impulse (curves 2–4) increases the magnitude of the maximum and shifts it to lower frequencies.

For the case of random orientation we have

$$\vec{P}^*(\omega) = \vec{P}_E \pi^{1/2} \omega \Delta t \exp\left[-\left(\frac{\omega \Delta t}{2} \right)^2 \right] \times$$
$$\times \left[1 + \frac{L}{l_c} \frac{1}{(1 + (\omega\tau)^2)^{1/2}} \right] . \qquad (22d)$$

In obtaining this result we assumed that the contribution from grains located at distance r from the crack is proportional to $[N(r)]^{1/2}$, where $N(r)$ is the number of such grains, given by approximately by $4\pi r^2/l_c^2$. Figure 4e shows that including the seismic impulse increases the low frequency part of the spectrum. Comparison of the spectra of the various sources considered here (Figures 4(a–e)) shows that piezomagnetic and electrokinetic sources activate the low-frequency EM modes while a piezolectric source activates the high-frequency modes. Note that in most cases the contribution of an acoustic impulse generated by a crack is much larger then the contribution of the crack itself.

Even for these simplified spectral densities, however, an exact solution for the radiation fields would require a more accurate solution to the monochromatic problem, over all frequencies, than is afforded by using the asymptotic formulas. Attempting such a solution would lie outside the scope of this paper. Nevertheless, based on our results so far, we can arrive at some qualitative conclusions concerning the shape and behavior of an electromagnetic pulse propagating along the earth's surface.

For $\omega_{\max} \ll \omega_h$, attenuation is very small, as noted above. In particular, the shape of the radiation pulse observed at the surface will be similar to that of the dipole pulse and, therefore, of the mechanical pulse producing it. Its intensity will fall off as some inverse power of the distance from the hypocenter.

For $\omega_{\max} > \omega_h$, which is the usual case, attenuation will be small in the frequency range $0 < \omega < \omega_h$ but will be significant in the range $\omega > \omega_h$. The shape of the radiation pulse will be altered by this dispersion. With increasing distance from the hypocenter, the pulse will broaden and become oscillatory in addition to becoming weaker.

E. Magnitude of Magnetic and Electric Dipole Moments

Now let us determine the electric and/or magnetic dipole associated with various mechanical sources. To do this we need to assume that the strain tensor is a given function of space and time. This tensor can always be represented as the sum of a pure volume strain (diagonal components only) and a pure shear strain (off-diagonal components only). For example, in an isotropic medium,

$$\varepsilon_{ij} = \begin{pmatrix} \theta & 0 & 0 \\ 0 & \theta & 0 \\ 0 & 0 & \theta \end{pmatrix} + \begin{pmatrix} 0 & \varepsilon & 0 \\ \varepsilon & 0 & 0 \\ 0 & 0 & 0 \end{pmatrix} ,$$

where θ and ε are the volume and shear strains, respectively. For either type of strain, the spatial dependence can be considered to be some linear combination of a unipolar and a bipolar square pulse (Figure 5). Thus for a shear strain,

$$\varepsilon = [\varepsilon_{\rm up}(H(x + l_c/2) - H(x - l_c/2)) +$$
$$+ \varepsilon_{\rm bp}(H(x + l_c/2) - 2H(x) +$$
$$+ H(x - l_c/2))] \cdot [H(y + l_c/2) -$$

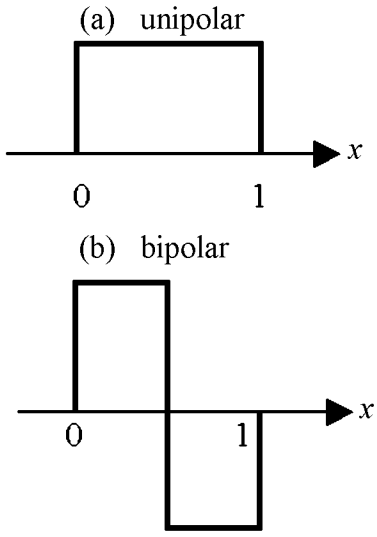

Figure 5. Square pulses of width l: (a) unipolar pulse; (b) bipolar pulse.

$$- H(y - l_c/2)] \cdot [H(z + l_c/2) - H(z - l_c/2)] ,$$

where $\varepsilon_{\rm up}$ and $\varepsilon_{\rm bp}$ are the magnitude of the unipolar and bipolar shear strains respectively. A similar expression can be written for the volume strain θ.

Based on the expressions for $\varepsilon(\omega, r)$ and $\theta(\omega, r)$ and on the formulas of this section and the previous section (Equations 21(a′, b′,c′), 17(a–d), 10–14 and A9), the magnetic and electric dipoles for various sources, after integrating over the spatial coordinates, are presented in Table 2 in terms of the parameters of the mechanical disturbance.

From this table we see that a piezomagnetic source produces a magnetic dipole for a unipolar pulse, while a piezolectric source produces an electric dipole for a unipolar pulse. An electrokinetic source produces an electric dipole for a unipolar pulse volume strain. An induction source produces a magnetic dipole for a bipolar pulse and an electric dipole for a unipolar pulse.

Now we have all the formulas necessary to estimate the electromagnetic field at the earth's surface due to a mechanical disturbance in the earth's crust. The relevant equations and the various cases to which they apply are summarized in Table 3.

F. Relation Between Measured and Actual Fields at the Detector

So far in this section we have considered the temporal and spatial distribution of the electromagnetic field from an impulse source. To compare with measurements we must consider how the real EM field at the detector is related to what the detector records. The latter depends on the measurement technique and the detector parameters.

Usually any detector of electromagnetic emissions will have two distinct parameters, the frequency channel and the

Table 2. Magnetic and electric dipole moments for various sources

Source \ Dipole type		Magnetic dipole		Electric dipole	
		Unipolar	Bipolar	Unipolar	Bipolar
	V.S.	M_{MV}	0	0	0
Piezomagnetic	S.S.	M_{MS}	0	0	0
	V.S.	0	0	P_{EV}	0
Piezolectric	S.S.	0	0	P_{ES}	0
	V.S.	0	0	P_{KV}	0
Electrokinetic	S.S.	0	0	0	0
	V.S.	0	M_{IV}	P_{IV}	0
Induction	S.S.	0	M_{IS}	P_{IS}	0

$M_{MV} = 2\mu I\chi_{||} l^3\theta$ $\qquad$ $P_{EV} = \mu D l^3\theta$

$M_{MS} = \mu I\chi_{||} l^3\varepsilon$ $\qquad$ $P_{ES} = 2\mu D l^3\varepsilon$

$M_{IV} = \frac{1}{8} C_l F\sigma l^4\theta$ $\qquad$ $P_{KV} = \sigma l^2(C_1 - C_2)K_2(\beta/\beta')\theta$

$M_{IS} = \frac{1}{8} C_t F\sigma l^4\varepsilon$ $\qquad$ $P_{IV} = C_l F\sigma l^3\theta$

$P_{IS} = C_t F\sigma l^3\varepsilon$

Note: V.S.=Volume strain and S.S.=shear strain; for simplicity the subscripts "up" and "bp" have been ommited from θ and ε but from the table it should be clear which type of pulse applies.

acquisition time. We characterize the frequency channel by a filtering function $g(\omega)$ and denote the acquisition time by ΔT. If we denote by E_m the mean electric field recorded by the detector, and by $E_f(t)$ the filtered electric field at the detector at time t $(0 < t < \Delta T)$, then

$$E_f(t) = \frac{1}{\pi}\int_{-\infty}^{\infty} E(\omega)g(\omega)e^{i\omega t}d\omega \tag{23}$$

and

$$E_m = \left[\frac{1}{\Delta T}\int_0^{\Delta T} E_f(t)F_f^*(t)dt\right]^{1/2}, \tag{24}$$

where $E(\omega)$ is the fourier component (i.e. spectral density) at frequency ω of the source electric field at the location of the detector. Using Equations 23 and 24 and doing the integration over t, we can express E_m as

$$E_m = \left[\frac{1}{4\pi^2\Delta T}\int_{-\infty}^{\infty} d\omega E^*(\omega)g(\omega) \times \right.$$
$$\left. \times \int_{-\infty}^{\infty} d\omega' E(\omega')g(\omega')\frac{e^{i(\omega-\omega')\Delta T}}{i(\omega-\omega')}\right]^{1/2}. \tag{25}$$

For simplicity we take

$$g(\omega) = H\left[\omega - \left(\omega_0 + \frac{\Delta\omega}{2}\right)\right] -$$
$$-H\left[\omega - \left(\omega_0 - \frac{\Delta\omega}{2}\right)\right],$$

i.e. a frequency window of width $\Delta f = \Delta\omega/2\pi$ centered at frequency $f_0 = \omega_0/2\pi$. We suppose that $\Delta f \ll f_0$. This is the usual case experimentally.

We will assume the duration Δt of the impulse to be small enough that $(\Delta t)^{-1} \gg \omega_0$; thus we expect the spectral density $E(\omega)$ to be a slowly varying function of ω in the neighborhood of ω_0. This will be used in integrating Equation 25.

Let's consider two quite different cases. In the first case, $(\Delta T)^{-1} \ll \Delta\omega \ll \omega_0$, while in the second case $\Delta\omega \ll (\Delta T)^{-1} < \omega_0$. In the first case, integration of Equation 25 yields

$$E_m \approx \left[\frac{\Delta\omega}{4\pi\Delta T}E(\omega_0)E^*(\omega_0)\right]^{1/2}, \tag{26a}$$

while in the second case we get

Table 3. The numbers of the relevant equations used and the cases to which they apply

	$r < r_A$	$r_A < r < r_B$	$r_B < r < r_C$	$r > r_C$
$\omega < \sigma/\varepsilon$	18(a–d)	$B1 - B6$	$B7 - B8$	$B9 - B10$
		$B11 - B16$	$B17 - B18$	$B19 - B20$
		$B21 - B23$	$B24 - B25$	$B26 - B27$
		$B28 - B30$	$B31 - 32$	$B31 - B32$
$\omega > \sigma/\varepsilon$	$r < r_B$		$r > r_B$	
	19(a–d)		20(a–d)	

$$E_m \approx \left(\frac{\Delta\omega}{2\pi}\right)\left[E(\omega_0)E^*(\omega_0)\right]^{1/2} \ . \tag{27a}$$

Suppose that during the time $\Delta T \gg \Delta t$ there are N electric impulses randomly distributed in time which appear at the measurement point. Then it is easy to show that the average field from N equal impulses scales as $N^{1/2}$, as a consequence of their random nature. In this case Equations 26a and 27a yield

$$E_m \approx \left[\frac{\Delta\omega N}{4\pi\Delta T}E(\omega_0)E^*(\omega_0)\right]^{1/2} \ , \tag{26}$$

$$E_m \approx \left(\frac{\Delta\omega}{2\pi}\right)\left[NE(\omega_0)E^*(\omega_0)\right]^{1/2} \ . \tag{27}$$

The preceding discussion can be carried through for the magnetic field, with completely analogous results. The first case results in

$$B_m \approx \left[\frac{\Delta\omega N}{4\pi\Delta T}B(\omega_0)B^*(\omega_0)\right]^{1/2} \ , \tag{28}$$

and the second case in

$$B_m \approx \left(\frac{\Delta\omega}{2\pi}\right)\left[NB(\omega_0)B^*(\omega_0)\right]^{1/2} \ . \tag{29}$$

We thus obtain two different formulas for the measured field E_m (or B_m). If $\Delta f = \Delta\omega/2\pi = 10^3$ Hz and $\Delta T = 10$ s, the relative magnitudes of E_m (or B_m) from the two expressions (26) and (27) (or (28) and (29)) is $(\Delta f \Delta T)^{1/2} = 100$. The reason for this difference requires some clarification. In Equations (26) (or (28)), the detector accumulate the energy throughout the time ΔT. If the source is emitting in an impulse mode, with a pulse width $\Delta t \ll \Delta T$, there is a considerable amount of "dead time", during which the detector receives no signal. This reduces the average signal considerably. In Equations (27) and (29) we suppose that $\Delta\omega \ll (\Delta T)^{-1} < \omega_0$, which means that the detector is receiving a signal throughout its acquisition time. This is why ΔT does not appear in Equations 27 and 29 and a much lager signal is measured (for an impulse source).

For both E_m and B_m, we will see later in Section 5 that the two cases imply two different measurement techniques, and the probability of detecting an observable SEM anomaly may depend critically on which technique is used.

5. Interpretation of Field Experiments

During the past century a wealth of SEM data has accumulated which has been interpreted as having some relation to pre-seismic processes. We want now to apply our model to the interpretation of some of this data. The search for SEM anomalies has spanned a wide frequency range from quasi-static (periods of weeks or months) up to radio frequencies (<50 MHz). Both magnetic and electric fields have been measured, using detectors below ground as well as above ground. A partial list of the types of anomaly which have been reported includes

- tectonomagnetic – local quasi-static changes of the geomagnetic field
- electrotelluric – local quasi-static changes of the electrotelluric field over periods of week, hours or minutes
- magnetic fluctuations in the ultra-low frequency (ULF) range, 10^{-2} to 10 Hz
- electromagnetic emission in the RF range, 1 kHz to 50 MHz.

We will estimate and compare with reported data the magnitude of the various types of SEM anomaly.

A. Tectonomagnetic Anomalies

This type of field experiment has a very long history. Occurrences of very large anomalies were observed centuries ago [*Rikitake,* 1976a, 1976b]. These early effects were reported to be comparable in magnitude to the geomagnetic field. However, as Rikitake has jokingly commented, the magnitude of reported anomalies seems to have fallen off exponentially with time, so the present day anomalies are some four orders of magnitude smaller, i.e. of order 1–10 nanotesla (nT). The typical duration time, T, varies from days to month, but there have been reports of T as small as minutes [*Johnston,* 1989; *Moore,* 1964; *Mueller and Johnston,* 1998; *Shapiro and Abdullabekov,* 1982; *Shapiro et al.,* 1994; *Skovorodkin et al.,* 1978]. In those cases where tectonomagnetic anomalies are followed by quakes, the elapsed time before the quake is comparable to T. Anomalies have been detected at distances up to 30 times the size of their origin. The general hypotheses put forth to explain these anomalies are based either on the piezomagnetic effect [*Sasai,* 1980, 1991; *Stacey,* 1964; *Stacey and Johnston,* 1972; *Zlotnicki and Cornet,* 1986] or the electrokinetic effect [*Fitterman,* 1978, 1979a; *Mizutani and Ishido,* 1976; *Mizutani et al.,* 1976].

First, let's estimate the size of the anomalous magnetic field assuming it originates from piezo-magnetism. Suppose we have some region of the crust, of linear extent ρ, located at distance R from the point of measurement, and that this region has piezomagnetic properties. Suppose further that during the duration time T of the anomaly a number N of cracks form in this region, with N given approximately by (see Equation 5)

$$N = \alpha\rho^3 n_{\max} \ . \tag{30}$$

The residual strain field around an isolated crack extends out to about three times the crack length (see Equation 1b). This leads to the appearance of a magnetic dipole, for the *ith* crack, of moment

$$\vec{M}_i^*(t) = \vec{M}^0(3l_i)^3 H(t - t_i) \ , \tag{31}$$

where t_i is the time of appearance of the *ith* crack (measured

from when the anomaly begins) and the components of $\vec{M}^0$ are given by Equation 10. From Equations 18a and 31 the cumulative effect is to create a magnetic field $\vec{B}$ whose magnitude is given approximately by

$$\vec{B} = \frac{\mu}{4\pi} \sum_{i=1}^{N} \vec{M}^0 \frac{(3l_i)H(t-t_i)}{R_i^3} \ .$$

For simplicity we assume that all cracks have the same length and orientation and have the same value of R. Then from Equations 4, 10 and 30 the magnetic field, after all N cracks have formed, becomes approximately

$$B = \frac{\mu}{4\pi}\alpha(\rho/R)^3 I \mu_s \chi_{||}\varepsilon \equiv \frac{\mu}{4\pi}\bar{\varepsilon}\mu_s\chi_{||}(\rho/R)^3 I \ . \qquad (32)$$

From this we see that the size of the magnetic anomaly is independent of crack size but proportional to the coefficient α or the average shear strain $\bar{\varepsilon}$, and strongly dependent on the ratio (ρ/R). The latter dependence means that the anomaly is stronger when it arises in a region close to the observation point. It also means that sources close to the observation point ($\rho/R \sim 1$) have a higher probability of being observed compared to distant sources (ρ/R ranging from 1/10 to 1/30). We expect this statement to be valid even when the density of cracks in nearby regions is low (small α or $\bar{\varepsilon}$) compared, for example, to the high crack density near the focal point of a distant quake. Estimating the strain $\bar{\varepsilon}$ to be 10^{-4} to 10^{-5}, setting $\rho/R = 1$, and using values of $\mu_s, \chi_{||}$ and I from Tables 6 and 1, Equation 32 gives $B \approx$ 0.3–3 nT, which is comparable to the observed data.

The model based on the electrokinetic effect was first proposed by *Mizutani and Ishido* [1976]. These authors noted the relation between local geomagnetic anomalies and the level of the water table during the Matsushiro earthquake swarm. Fitterman developed this model further [*Fitterman,* 1978, 1979a, 1981].

The magnetic field associated with a system of currents generated by an electrokinetic source has some characteristic features. It is known [*Fitterman,* 1978] that in any homogeneous medium with an arbitrary distribution of pressure variations due to pore water, the geomagnetic effect is zero. That is, the electric current due to the motion of the pore water is exactly cancelled by the current arising from the electric field which is created. A non-zero effect occurs only in an inhomogeneous medium, and its magnitude depends only on the degree of inhomogeneity. However, not all types of inhomogeneity will produce a geomagnetic effect on the earth's surface. For example, it can be shown that when the inhomogeneity is only in the vertical direction, i.e. in a horizontally stratified crust, there is no above-ground geomagnetic effect [*Fitterman,* 1978; *Gershenzon,* 1992]. But there will be an effect below the surface, and it will be greatest at the boundary between strata. So geomagnetic effects of an electrokinetic nature arising from geodynamic processes would be observed on the earth's surface only if there were inhomogeneities in the horizontal direction (e.g. faults or inclusions).

For the estimation of the magnitude of magnetic field disturbances, therefore, it makes sense to consider, as the simplest model, two media (medium 1 and medium 2) separated by a vertical boundary. In this case the magnitude of the magnetic field disturbance at the intersection of the boundary with the surface can be estimated by the simple formula [*Fitterman,* 1979a, 1979b]

$$B = \frac{\sigma_1\sigma_2\mu(C_1 - C_2)P}{2\pi(\sigma_1+\sigma_2)} f \ , \qquad (33)$$

where f is a dimensionless geometrical factor weakly dependent on the size of the boundary. For realistic cases f does not exceed 20 [*Gershenzon and Gokhberg,* 1992]. We shall use f=10. The pressure variation P arises from the appearance of multiple cracks in some regions. Expressing P in terms of θ, the change in the volume strain, via Equation A9, we obtain B for various values of $\theta, \sigma_1, \sigma_2$ and $C_1 - C_2$ (Table 4). This table shows that the magnetic disturbance becomes significant ($\sim$ 1 nT) only for changes in volume strain greater than 10^{-6} and conductivities greater than $10^{-2}/\Omega - m$.

Table 4. Estimate of the magnetic field (in nT) arising from an electrokinetic source, using Equation 33. Here $\sigma = \sigma_1 = \sigma_2$, $C_1 - C_2 = 10^{-6} - 10^{-7}$ V/Pa and $f = 10$

σ \ θ	10^{-4}	10^{-5}	10^{-6}	10^{-7}
10^{-1}	10–100	1–10	0.1–1	$10^{-2} - 10^{-1}$
10^{-2}	1–10	0.1–1	10^{-2}–10^{-1}	10^{-3}–10^{-2}
10^{-3}	0.1–1	10^{-2}–10^{-1}	10^{-3}–10^{-2}	10^{-4}–10^{-3}

We have not considered changes in water permeability or changes in the streaming potential, C, accompanying a preseismic process. These changes could affect the size of the geomagnetic anomaly. Changes in C are difficult to calculate because they are related to changes in the composition of the pore water. Changes in water permeability likewise are difficult to calculate but might be significant when the porosity is small and θ is large. The seasonal runoff of ground water in mountainous areas has been observed to give rise to a large electrokinetic current and magnetic field. For example, a pore pressure difference of 10^6 Pa over a horizontal distance ΔL of 100 m gives a pressure gradient dP/dx of 10^4 Pa/m, which results in a magnetic field $B = C\mu\sigma\Delta L dP/dx$ ranging from 10 to 100 nT for $\sigma = 10^{-1}/\Omega - m$ and $C = 10^{-7}$ to 10^{-6} V/Pa. A change of 10% in this field due to a pre-seismic process would give rise to an easily observable anomaly of 1 to 10 nT.

So both mechanisms, under appropriate conditions, can produce fields strong enough to be comparable to observed anomalies. However we emphasize that one of these conditions is that the distance from the point of measurement to the source be comparable to the size of the source.

We also note that there is a simple way of distinguishing which of these two types of sources, piezomagnetic or electrokinetic, is responsible for an observed magnetic anomaly, based on the temporal behavior of the latter. If the anomaly behaves approximately like a step function, i.e. shows a

residual field, then it is piezomagnetic in origin. If it behaves approximately as a unipolar pulse with no residual field, it is electrokinetic in origin.

B. Electrotelluric Anomalies

The search for earthquake precursors in the electrotelluric field extends back about eighty years. This search has been conducted in many areas of high seismic activity worldwide (Japan [*Fukutomi,* 1934; *Miyakoshi,* 1986; *Noto,* 1933; *Ozima et al.,* 1989; *Shiratori,* 1925; *Uyeda, et al.,* 2000], the former Soviet Union [*Sobolev et al.,* 1981], Greece [*Lighthill,* 1996; *Varotsos and Alexopoulos,* 1984a, 1984b, 1987; *Varotsos et al.,* 1993], China [*Qian et al.,* 1990; *Raleigh et al.,* 1977], Bulgaria [*Ralchovsky and Komarov,* 1987], USA [*Sornette and Sornette,* 1990]). Several hundred cases have been reported which relate such anomalies to strong nearby quakes. In general, the morphological features of these anomalies are defined by the region of occurrence and method of detection. The magnitude of the disturbances ranges from a fraction of a millivolt to a few tens of millivolts; it depends on the quake magnitude and distance from the epicenter but in many cases the magnitude is independent of the measurement line length. The duration of an anomaly can range from minutes to weeks and is only weakly dependent on quake magnitude and distance from epicenter.

The nature of these anomalies is not well known. There exist models based on the classical and non-classical piezoelectric effects discussed in Section 3B [*Gokhberg et al.,* 1985; *Slifkin,* 1996; *Sobolev and Demin,* 1980; *Varotsos and Alexopoulos,* 1986], and the electrokinetic effect (Section 3C) [*Bernard,* 1992; *Dobrovolsky et al.,* 1989; *Fitterman,* 1979b; *Gershenzon and Gokhberg,* 1989, 1993]. Sometimes the occurrence of anomalies has been ascribed to changes in the conductivity of the crust [*Meyer and Pirjola,* 1986]. In some cases they have been explained in terms of changes in the chemical composition of pore water around one or both of the measurement electrodes, giving rise to an apparent electrotelluric signal [*Miyakoshi,* 1986]. Such chemical changes could alter the ζ-potential of the double electric layer at the electrode-water interface.

We ask how pre-seismic processes relate to the appearance of an electrotelluric field at distances of tens to hundreds of kilometers from the epicenter. There are at least two alternative explanations.

The first one, preferred by most experimenters, supposes that somehow a large current is generated in the focal area and is distributed over a great distance to the detector. This explanation has not been confirmed in most cases. For example, *Yoshimatsu* [1957] used two parallel lines 100 m and 1500 m in length and the signal appeared only in the shorter line, whereas we would expect it to appear in both lines if the above explanation were true. *Noto* [1933] used two lines perpendicular to each other and the anomalous signals appeared in only one of them, which is again difficult to explain in terms of a large-scale current distribution, even in the presence of inhomogeneities in the conductivity. *Miyakoshi* [1986] described anomalies as close as 3 km from the epicenter of a 5.2 magnitude quake. He used three short lines, each 30 m long, in a geophysical tunnel, and two perpendicular lines on the ground, each 600 m long. He saw anomalous signals only in one of the short lines. They clearly exceeded normal levels and lasted about two months. If these signals were electrotelluric in origin, they certainly could not be explained in terms of a large-scale current system. The so-called $\Delta V/L$ test has been introduced to eliminate noise for short lines on VAN and similar networks. But there are examples where this test does not work on such networks [*Gershenzon and Gokhberg,* 1993; *Uyeda, et al.,* 2000].

In order to explain the appearance of SES generated by pre-seismic processes in the focal area but located hundreds of km from this area, *Varotsos et al.* [1998] proposed the existence of a special *pencil-like* region of high conductivity in the crust, extending from the dipole and terminating at the field point. Although regions of strong inhomogeneity are not unusual in the crust, we think the existence of this special *pencil-like* form extending for several hundreds of km and terminating very close to the detector is unrealistic. Calculations by *Bernard* [1992] also support this conclusion.

The inadequacy of the explanation in terms of a large-scale current system originating in the focal area leads us to the second alternative, namely, a large-scale mechanical stress field which can, under certain condition, produce electrotelluric anomalies *locally.* Then the morphological features of the anomalies represented by the several examples cited in the previous paragraph can be explained in terms of the electrokinetic effect [*Bernard,* 1992; *Dobrovolsky et al.,* 1989; *Gershenzon and Gokhberg,* 1989, 1993]. As mentioned before, the current distribution created by an electrokinetic source in a homogeneous medium is zero on a scale larger than the individual grains. Non-zero currents will appear only on the boundary separating two homogeneous components of an inhomogeneous medium. Across this boundary, the electric potential will be discontinuous, and two electrodes placed on opposite sides of the boundary will show a voltage practically independent of the distance between the electrodes. This voltage will depend on the strength of the electrokinetic source and the electrical characteristics of the two components. This would explain why the anomalous signals are selective and why the strength of an anomalous signal is sometimes independent of the length of its measurement line.

The typical pore pressure relaxation time depends on the size and shape of the disturbed region and can range from minutes to hours, days or weeks, which coincides with the time range over which electrotelluric anomalies are observed to occur. No single mechano-electromagnetic mechanism involving the crystal matrix of the rocks, e.g. piezomagnetic or piezolectric (classical and non-classical), could act over such large time scales, because the formation time for such disturbances is only 1 second or less, i.e. of the order of the linear extent l of the region divided by the elastic wave velocity. Once formed, such disturbances dissipate with a time constant $\mu\sigma l^2$ which is even smaller.

Let's calculate the magnitude of the electrotelluric field from an electrokinetic source. The maximum effect occurs when the two electrodes span an inhomogeneity. In this case

Table 5. Electrotelluric potential $\Delta\phi$ in mV calculated using the electrokinetic model for a range of volume strains and streaming potential inhomogeneities. The parameters β, β' and K_2 in Equation 34 are given in Table 6

$C_1 - C_2$(V/Pa) \ $\bar{\theta}$	10^{-4}	10^{-5}	10^{-6}	10^{-7}	10^{-8}
10^{-6}	1000	100	10	1	10^{-1}
10^{-7}	100	10	1	10^{-1}	10^{-2}

the potential difference $\Delta\phi$ can be expressed by

$$\Delta\phi = (C_1 - C_2)P = (C_1 - C_2)\frac{\beta K_2}{\beta'}\bar{\theta} \ . \tag{34}$$

In Table 5 we tabulate $\Delta\phi$ for a range of $\bar{\theta}$ and $C_1 - C_2$.

Table 5 shows that strains exceeding the tidal value (10^{-8}) can be detected, but only under the following conditions:

- water-saturated crustal material near the surface
- a vertical strong inhomogeneity in the electrokinetic parameters
- placement of the electrodes so as to bridge the inhomogeneity.

This model explains in a natural way the strong selectivity of electrotelluric anomalies.

In spite of the fact that no macroscopic electric current will exist in a homogeneous medium, an electric field can exist and is measurable. In a homogeneous medium the potential between points 1 and 2 is $\Delta\phi = C(P_1 - P_2)$. Normally, if the electrodes are at the same depth the difference between P_1 and P_2, and hence $\Delta\phi$, is negligibly small. But if the electrodes are at different depths (for example, one above and one below the water table) a significant potential can arise.

Consider a simple example. Suppose at t=0 a step-function change in volume strain (and resulting pore pressure) occurs in the vicinity of two electrodes placed in a homogeneous medium. If $P_1 = P_2$ after the change, then $\Delta\phi$ remains zero. But if the environment around the two electrodes is slightly different, leading, for example, to different water permeabilities or different distances between the electrode and the water table level, the pressures P_1 and P_2 will relax back to their equilibrium values at different rates, leading to a spike in P_1 and P_2 at some time $t > 0$. In such a case the duration of the anomaly does not depend on the source but on the local environmental differences between the electrodes. The theoretical shape of the spike coincides with the shape usually observed, in the SES reported by the VAN group. In addition, when several signals are observed their duration is usually the same, in agreement with this simple model.

The above example indicates that if, instead of offsetting the electrodes horizontally, they are offset vertically above and below the water table, the electrotelluric anomaly in a homogeneous medium might be maximized. In such an experiment it was shown that a good correlation existed between the electrotelluric field and tidal deformation [*Gershenzon et al.,* 1990]. So under some conditions this method of measuring the electrotelluric field can be extremely sensitive. The use of a short vertical baseline also serves to reduce background noise. This method does have the disadvantage that it cannot detect an electrotelluric disturbance unless the electrodes are in a region where the volume strain is changing.

We have shown how placing the electrodes within a source of mechanical disturbances can yield detectable electrotelluric fields, even when the source is as weak as tidal deformation. Now we consider the situation where the electrodes are placed outside the source. For purposes of estimating the effect we use Equation 18b, which gives the electric field associated with a static electric dipole. Setting h=0 and y=0 for simplicity, and using P_{KV} from Table 2 (with $\bar{\theta}$ in place of θ) for the dipole moment P^* associated with an electrokinetic source, we have

$$E \cong \frac{l^2(C_1 - C_2)\beta K_2 \bar{\theta}}{\pi R^3 \beta'} \ . \tag{35}$$

The field varies as l^2, the area of the vertical inhomogeneity, and inversely as the cube of the distance R between source and detector. In Figure 6 we show how E varies with R (logarithmic scale) for $\bar{\theta}$ equal to 10^{-4} and for a range of l (10 m to 10 km), based on the above formula.

The range of applicability of the dipole approximation limits R to values larger than about $3l$, so the graphs in Figure 6 do not extend down to values of R which are below this limit. Even for a source comparable in size to the origin of a large earthquake (1 km $\leq l \leq$10 km), Equation 35 gives a field at a distance of 100 km from the source which is three to five orders of magnitude less than the reported anomalies. Incorporating the effects of inhomogeneities in the conductivity in the crust could increase the field by several times, but it is highly unlikely to increase it by three to five orders of magnitude.

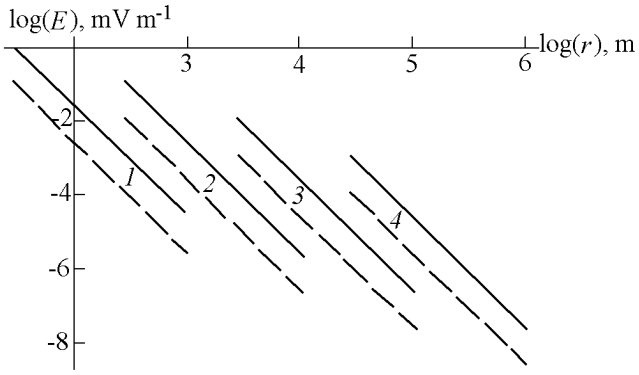

Figure 6. The quasi-static electric field as a function of distance for various electrokinetic source sizes l. $\bar{\theta} = 10^{-4}$, remaining parameters from Table 6. Dashed lines: $C_1 - C_2 = 10^{-7}$ V/Pa; solid lines, $C_1 - C_2 = 10^{-6}$ V/Pa. (1) l = 10 m, (2) l = 100 m, (3) l = 1 km, (4) l = 10 km.

For a small source (l=10 and 100 m) the field is detectable at distances close to the source, as seen in Figure 6. The graphs for l=1 km and l=10 km correspond to co-seismic effects. These are negligibly small, which is consistent with their absence in electrotelluric field measurements far from the epicenter. Here the term "co-seismic" refers to EM signals generated at the focal area during the main shock, and not to seismic waves.

Consideration of the possible physical mechanisms for electrotelluric anomalies leads to the conclusion that the electrokinetic effect is the most appropriate candidate.

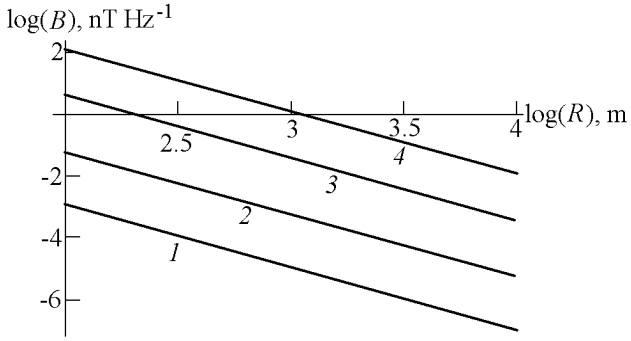

Figure 7. Variation of magnetic field B_m with distance R from an electrokinetic source, for four combinations of crack size and channel frequency. (1) l_c = 1 m, f_0 = 7.5 Hz; (2) l_c = 2 m, f_0 = 0.751 Hz; (3) l_c = 5 m, f_0 = 0.073 HZ; (4) l_c = 10 m, f_0 = 0.015 Hz. Parameter values are $\alpha = 1, \theta = 10^{-2}, C_1 - C_2 = 10^{-6}$ V/Pa, ΔT = 1800 s, $\sigma = 10^{-1}/\Omega - m$ and ρ = 100 m. Remaining parameters from Table 6.

C. Electromagnetic Emission in the Ultra-Low Frequency Range

A few observations of anomalous electromagnetic emission in the ultra-low frequency (ULF) range (10^{-2}–10 Hz) have been reported. In 1964 two articles appeared dealing with the detection of anomalous magnetic impulses before an earthquake [*Breiner,* 1964; *Moore,* 1964]. The duration of these impulses indicated the disturbance was in the ULF range. The report by *Fraezer-Smith et al.,* [1990] stimulated more interest in this field. This article reported ULF disturbances in the geomagnetic field before and after the magnitude 7.1 Loma Prieta earthquake. These disturbances appeared more than one month before the quake and were detected over several frequency channels. The most intense disturbance, in the range 0.1 to 0.2 Hz, began approximately three hours before the quake and exceeded background by two orders of magnitude. Analysis of the data indicated that it was not due to magnetic fluctuations in the earth's upper atmosphere nor to quake-induced detector motion. The authors concluded that the intense ULF disturbance was probably a magnetic precursor. Anomalies in the ULF range have also been reported in other seismically active regions [*Fujinawa and Takahashi,* 1998; *Hayakawa et al.,* 1996; *Kopytenko et al.,* 1993].

Several models have been developed to explain the geomagnetic phenomena associated with the Loma Prieta quake. The first was based on the induction effect [*Draganov et al.,* 1991]. However, it was shown by others that this model requires unrealistic conditions, such as very large changes in the volume strain and a pore water pressure exceeding lithostatic values [*Fenoglio et al.,* 1995; *Gershenzon and Gokhberg,* 1994]. On the other hand, using the same parameters as in the induction model, the electrokinetic effect has been shown in Section 3 and in the paper by *Gershenzon and Gokhberg* [1994] to give a magnetic disturbance three to five orders of magnitude greater than the induction effect.

The model using the electrokinetic effect was developed by *Gershenzon and Gokhberg* [1994]. It was shown that multiple cracks appearing in a sub-surface layer could account for the observed effect. This model was able to explain the frequency dependence as well as the magnitude. *Fenoglio et al.,* [1995] presented a model, also based on the electrokinetic effect, with a more developed mechanical component, i.e. they showed that the source of the pore pressure gradient could be "failure of faults containing sealed compartments with pore pressures ranging from hydrostatic to lithostatic levels". A similar idea was proposed earlier by *Bernard* [1992]. The pressure gradient in this case would be much larger than for the changes in the volume strain considered by *Gershenzon and Gokhberg* [1994]. The model of *Fenoglio et al.* [1995] could account for the observed effects at great distances from the mechanical source. *Merzer and Klemperer* [1997] proposed a model based on local conductivity changes in the earth's crust. In the presence of normal external geomagnetic variation, conductivity changes in the crust could lead to local changes in the magnitude of the geomagnetic variation. However, the proposed geometry of the region necessary to account for the effect, i.e. an infinite horizontal elliptic cylinder of diameter several kilometers and instantaneous changes in the conductivity of several orders of magnitude, extending throughout this region, seems to us to be unrealistic. If the region of high conductivity were not infinite, the electric field arising in this region, and the resulting geomagnetic disturbance, would be much less. *Molchanov and Hayakawa* [1998] developed a model based on the formation of multiple cracks in the focal area during the earthquake formation stage. Since crack formation is accompanied by electric charge separation (due to various mechanisms) an EM field will appear. The low frequency part of this field could reach the surface. We find that the energy associated with charge separation during crack formation is distributed over a broad frequency range and only a small part occurs in the ULF region. Our model also considers the formation of multiple cracks (not necessarily restricted to the focal area), and we find that the electrokinetic effect is a mechanism which provides considerably more energy in the ULF range, because it is controlled by the diffusion of water with a diffusion time comparable to the period of ULF emissions.

So from the point of view of our model, geomagnetic anomalies in the ULF range could appear as the result of the action of multiple cracks via the electrokinetic effect. Consider, for example, a water- saturated crustal layer ex-

isting underneath the detector, with a number N of cracks appearing in the layer due to pre-seismic processes. The magnitude of the ULF field, B_m, could be calculated using Equations 28, 19b and 18c (with $h = y = 0$), Table 2 (with $l = l_c$), and with

$$N = \alpha n_{\max}(4/3)\pi\rho^3 = \frac{4\pi\alpha\rho^3}{3(3l_c)^3} \ ,$$

where the active region during the acquisition time ΔT is assumed to be a sphere of radius ρ. Figure 7 shows the variation of B_m with distance R from the source, for four different combinations of crack size and frequency. It is known that the crack size defines the spectral density of the signal through the diffusion relaxation time ΔT_D and seismic impulse life time τ. From Figure 7 we see that a 1m crack could account for the disturbance in the 5 to 10 Hz channel associated with the Loma Prieta quake, and a 20 m crack could account for the 0.01 to 0.02 Hz channel (see *Gershenzon and Gokhberg* [1994] for a more extensive discussion). In summary, Figure 7 shows that the Loma Prieta data could be accounted for by a local source lying within a water saturated layer and located within 1 km of the detector.

D. Electromagnetic Emission in the RF Range

Over thirty years ago, Vorobyev proposed that earthquakes are the result of an electromagnetic storm within the crust. Although this hypothesis must be rejected on theoretical grounds, since the electrical conductivity in the crust is too high for charge separation to occur over the large distances required, experiments to detect RF emission at the surface before and during a quake have been performed for several years in Uzbekhistan by Vorobyev and collaborators [*Mavlyanov et al.,* 1979; *Vorobyev et al.,* 1975, 1976]. The same type of experiments were also conducted in Carpathia [*Sadovsky et al.,* 1979] and the Caucasus [*Gokhberg et al.,* 1979].

A Russo-Japanese collaboration resulted in further experiments in Japan [*Gokhberg et al.,* 1982]. The authors reported intense electromagnetic emission (EME) at 81 kHz beginning 1.5 hours before a major quake (magnitude 6.1). The EME activity increased steadily with time until the main shock occurred, when it decreased abruptly. Twenty minutes later a large aftershock occurred and the EME activity decreased abruptly again, falling to the background level. This experiment initiated similar experiments in the RF range by several groups in various countries. One group in Japan reported twenty such occurrences over a two-year period [*Oike and Yamada,* 1994; *Oike and Ogawa,* 1986]. This group used a frequency of 163 kHz because of the low background activity at this frequency at their location. The associated quakes were all centered in Japan, had magnitudes greater than 6.0, and the EME was from four to twelve times background. Some evidence of EM emission relating to earthquakes in America also have been reported [*Tate and Daily,* 1989; *Warwick et al.,* 1982]. Anomalies at 3 and 10 kHz and 41 and 54 MHz were observed before several earthquakes in Greece [*Eftaxias et al.,* 2000, 2001; *Varotsos et al.,* 1996b]. Further references to field experiments in the RF range may be found in *Gokhberg et al.* [1995].

It is difficult to compare the results of the several groups working in this area because of differences in detectors, frequency ranges, and discrimination techniques. Nevertheless there are some common morphological features of the phenomenon:

- it shows some relation to the time of occurrence of large crustal quakes;
- the precursor times, of duration hours to days, are virtually independent of quake magnitude;
- the activity level is usually several times background;
- the larger the quake, the greater the distance from the hypocenter at which the EME can be detected.

EME noise in the RF range can have several sources, some natural (e.g. atmospheric lightning) and some man-made (e.g. commercial radio broadcasting, industrial activities). These sources are all hard to eliminate, because multiple reflections from the ground and the ionosphere can cause a signal to propagate over large distances.

We now discuss possible models for EME anomalies. The simplest model identifies the EME source with the origin of the quake, and requires a mechano-electromagnetic transducer of some kind which is active only during the precursor period. A serious flaw in this model is that it requires an attenuation length for RF signals which is on the order of the typical depths at which quakes originate. It is easy to show that the attenuation length in the crust is much less than this.

Another model was developed by *Gokhberg et al.* [1985]. It involves the creation of a large-scale electrical current, of very low frequency, which extends to the earth's surface. The electric field associated with this current loop, though weak, could extend into the atmosphere and produce a lightning discharge at high altitude, where the ionization potential becomes small. The lightning discharge could be a source of secondary emission in the RF range. The idea that atmospheric processes could be a source of EME has also been considered by *Fujinawa et al.* [1997].

Sadovsky et al. [1979] suggested that electromagnetic anomalies were related to changes in the electrical characteristics of the environment about the measurement point. These changes could be related to pre-seismic processes, while the source of the electromagnetic fields could simply be background noise.

Malyshkov et al. [1998] proposed a model in which the earth's crust constantly emits EM signals associated with background elastic waves. These signals would normally be part of the background EM noise, but a change in these signals, i.e. an EME anomaly, could occur when an elastic wave propagates through the altered mechanical state of an earthquake preparation region (i.e. an altered stress state or an altered density of microcracks). However this model is based on laboratory experiments in the ultrasound range (kHz to MHz). It is difficult to see how an EM signal in the RF range could be produced by the low-frequency seismic waves (10^{-2} to 10 Hz) observed in field experiments.

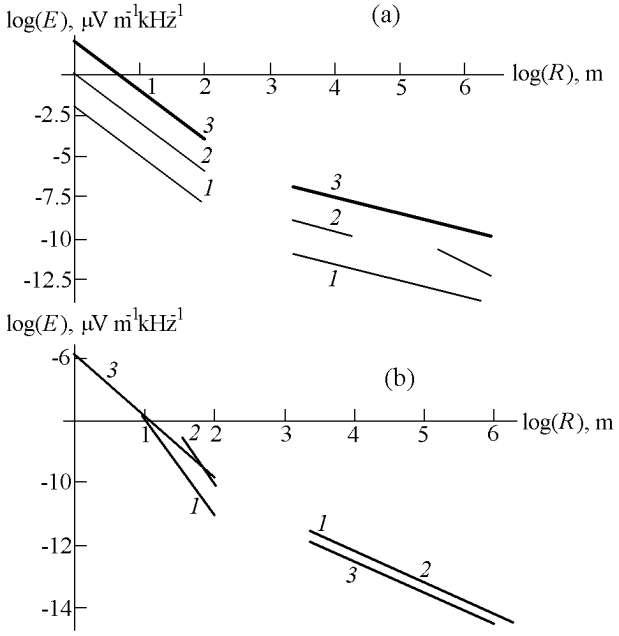

Figure 8. Variation of electric field E_m with distance R at channel frequency 10^5 Hz, for a single microcrack ($l_c = 10^{-3}$ m), due to (a) piezoelectric and (b) piezomagnetic sources. (1) $\sigma = 10^{-1}/\Omega - m$; (2) $\sigma = 10^{-3}\Omega - m$; (3) $\sigma < 10^{-4}/\Omega - m$. The breaks in the curves correspond to the limits of applicability of the asymptotic formulas (cf. Figures 2b, c).

From our viewpoint, the model developed here provides a natural framework for discussing the above RF phenomena. We will calculate the magnitude of the anomalies and discuss the circumstances under which they can be detected. But first we consider two different techniques which are applied in field experiments for monitoring SEM anomalies in the RF range. The first technique (simple averaging) is the usual one, in which all signals received during the acquisition window ΔT are averaged, and leads to Equations (26) and (28). The second technique (which we shall call impulse averaging) is based on the supposition that the useful signals (as opposed to noise) are pulsed rather than continuous. In this technique only filtered signals above a present threshold are considered. In this case, the time between impulses (the "dead time") does not influence the measurement. This technique corresponds to Equations (27) and (29) when ΔT is large enough to count one pulse or a cluster of closely spaced pulses but small enough to exclude the dead time. As we mentioned at the end of Section 4, the ratio of E_m (or B_m) calculated using pulse averaging to E_m (or B_m) using simple averaging is of order $(\Delta f \Delta T)^{1/2}$, which can be very large for reasonable values of Δf and ΔT (here ΔT is the acquisition time for simple averaging). This means that impulse averaging can be much more sensitive than simple averaging in detecting RF anomalies, in agreement with RF field experiments [*Gokhberg et al.,* 1986]. In the remainder of this section we shall present results based on the impulse averaging technique.

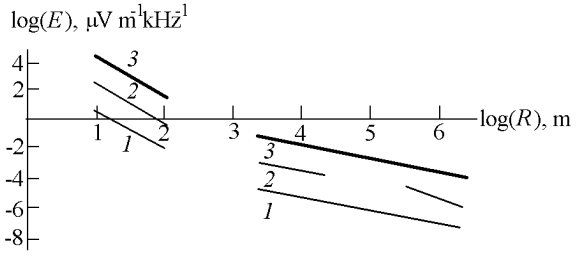

Figure 9. Variation of electric field E_m with distance R for N microcracks, where $N = \alpha\rho^3 n_{\max}$. Parameters used are the same as in Figure 8a, with $\alpha = 1$ and $\rho = 10$ m.

Figure 8 contains the results of calculations of E_m (Equation 27a) in the neighborhood of f=10^5 Hz generated by one microcrack, due to piezolectric (Figure 8a) and piezomagnetic (Figure 8b) sources. From the figure we see that the magnitude of E_m from a piezolectric source is several orders greater than that from a piezomagnetic source. This would seem to contradict the result of Section 3, where it was shown that the strengths of these two types of source are comparable. Actually there is no contradiction. The energy in a piezomagnetic source is distributed over a much broader frequency range than that for a piezolectric source (see Figures 4a and 4d). For the high end of the RF range, this means that a piezolectric source gives a much stronger signal, while at the low end the contribution of a piezomagnetic source could dominate.

From laboratory experiments and calculations it is apparent that the emission of one microcrack with typical size 1mm produces a very weak signal at distances greater than several meters (see Figure 8). From the standpoint of a field experiment this means that emission from a single microcrack will be below the threshold of the detector. However during the failure of a large portion of rock (i.e. larger then typical grain sizes) a large number of microcracks are formed in a short period of time. Their combined effect could produce a signal large enough to exceed detector threshold. Figure 9 shows the result of calculating E_m using Equation 27, based on a piezolectric source. In using Equation 27 we suppose that during the acquisition time N microcracks appear, where $N = \alpha\rho^3 n_{\max}$ and the failure region is assumed to be a cube of side ρ. From this figure we see that, at a given distance R, E_m increases with decreasing conductivity σ up to a value corresponding to $\sigma_0 = \omega\varepsilon$. For $\sigma < \sigma_0$, E_m is independent of σ. The quantity E_m has an inverse power law dependence on R; this power law changes from zone to zone. For $\sigma > \sigma_0$ (cf. Figure 2b) the dependence is R^{-3} for the static and near zones, R^{-1} for the intermediate zone, and R^{-2} for the far zone. For $\sigma < \sigma_0$ (cf. Figure 2c) the power law is R^{-3} for the near zone and R^{-1} for the far zone.

By use of the equations and figures presented here, we see that our model can explain the appearance of RF anomalies of order 10–100 μV/m under the following conditions.

- the detector is located within a few kilometers of the source;
- the active region consists of quartz-containing rocks;

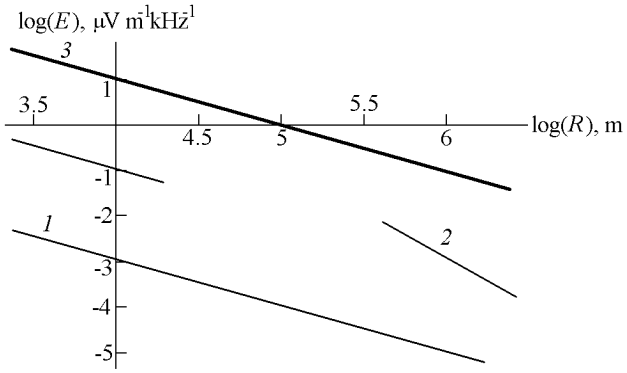

Figure 10. Variation of electric field E_m with distance R for N microcracks. Parameters used are the same as in Figure 9 except that $\rho = 10^3$ m.

- the conductivity of the active region is low (e.g. $\sigma \leq \sigma_0 \approx 10^{-4}(\Omega \cdot m)^{-1}$ for f=100 kHz).

This model cannot explain reported anomalies as large as 100 mV/m [*Mavlyanov et al.,* 1979; *Sadovsky et al.,* 1979; *Vorobyev et al.,* 1975, 1976]. Such anomalies may be related to atmospheric phenomena (lighting activity) connected with pre-seismic processes [*Fujinawa et al.,* 1997].

Figure 10 shows E_m calculated for a 1 km source (a typical size for an earthquake focal region). At distances greater than 10 km, the field is virtually undetectable. This means that processes at the focus cannot be responsible for RF anomalies occurring at a large distance from it.

6. Discussion and Conclusions

A. Major seismo-electromagnetic phenomena can be described by the following model. The final phase of the pre-earthquake process is accompanied by the formation of multiple cracks. Cracks appear not only in the focal area but also in a neighborhood. This occurs because regional geodynamic processes are connected by the global shear stress. The appearance of a crack creates, in its neighborhood, a mechanical disturbance over a broad frequency range. In general, the spectral density of the disturbance consists of two parts: a zero-frequency spike related to a change in the residual strain, and a broad region from zero up to the MHz range, related to an impulse-like process. In a crust saturated with water (the usual case), a crack will also cause a change in the pore water pressure, and the spectral density of this response is much less broad, extending from zero up to the range of kHz. Localized mechanical or pore pressure changes give rise to electromagnetic emission by a variety of mechano-electromagnetic transducer mechanisms. The emission will have a spectral density which spans the same range as its source.

B. The major known mechano-electromagnetic mechanisms which may be applied to the earth's crust, namely piezomagnetic, piezolectric, electrokinetic and induction, have been considered and are compared in Table 1a. From this table one can see that a piezomagnetic source has strength comparable to that of a pure quartz piezolectric source. In the case of high conductivity in the earth's crust, the strength of an electrokinetic source and a piezomagnetic source are also comparable. The magnitude of the induction effect is usually very small compared to the other three, but it could be comparable to them for a source of size 1 km or more.

C. Since the dimensions of the EM source are, in most real cases, much smaller than the distance from source to detector, all sources are represented by a magnetic or electric dipole. Formulas 21 and 22 and Table 2 express the magnitude of the electric and magnetic dipoles in terms of the parameters of both the earth's crust and the mechanical disturbances. The mechanical parameters important in calculations, namely strain spectral densities $\varepsilon(\omega, r)$ and $\theta(\omega, r)$, pore water pressure spectral density $P(\omega, r)$, crack density n, and average shear and volume strain changes $\bar{\varepsilon}$ and $\bar{\theta}$, are given in Equations 1c, 3a, 4, 5 and 5a. The relation between volume strain and pore water pressure is given by Equation A9.

Expressions 18(a–d) can be used for calculating the magnetic and electric fields in the so-called static zone and expressions B1–B32 in the near, intermediate and far zones for $\sigma/\omega\varepsilon > 1$. When $\sigma/\omega\varepsilon < 1$, expressions 19(a–d) and 20(a–d) can be used in the near and far zones, respectively. In order to connect the "detected" (filtered and averaged) EM field to the real field one uses expressions 26, 28 and 27, 29.

Collectively, all the above formulas represent the necessary relationships for estimating the measured EM field, at the detector, for a wide range of frequencies and at various distances from the source. Through them, the physical parameters of both the earth's crust and of a localized disturbance are connected to the measured EM field.

D. The magnitude and morphological features of major SEM phenomena have been interpreted on the basis of the model developed here.

1. Tectonomagnetic anomalies can be described either by the piezomagnetic or electrokinetic effect. In rocks containing titano-magnetite, residual strain as a result of the cumulative action of crack formation in a localized area can produce magnetic field variations of the order of nT. The same order of magnetic variation can be produced in water-saturated rocks of high electrical conductivity ($\sigma \geq 10^{-2}/\Omega - m$) by changes in pore water pressure. These two mechanisms can be distinguished by the temporal behavior of the magnetic variation (step-function behavior corresponding to the piezomagnetic mechanism and unipolar behavior corresponding to the electrokinetic mechanism).

2. Of the mechanisms considered in this paper, only the electrokinetic mechanism can explain the main features of electrotelluric field anomalies, namely duration, magnitude, and high degree of selectivity.

3. Geomagnetic variation in the ULF range may be explained on the basis of the electrokinetic effect, when the detector is located about a water-saturated layer which has a comparatively high conductivity. While the piezomagnetic effect could also contribute to the variation, the electroki-

netic effect is a more likely mechanism. The main reason for this is the difference in the spectral density of the mechanical disturbances associated with each. The energy of a piezomagnetic source is distributed widely from zero up to radio frequencies. The electrokinetic source is usually much narrower, with correspondingly much more energy in the ULF range.

4. The most powerful source of EME in the RF range is the piezolectric effect due to the presence of quartz grains in the crust. The magnitude of the piezomagnetic effect in the RF range is 2–3 orders of magnitude less.

E. Calculations based on the model presented here show that the source of all types of EM anomalies considered here should be *local*, i.e. close to the detector but not necessarily in the focal region, in order to be observed. The maximum distance from source to detector depends on the type of anomaly and on the detector, and can range from several hundred meters to several kilometers. One of the best experimental confirmations of this statement is the fact that there are no SEMS during earthquakes (excluding co-seismic signals accompanying seismic waves). An earthquake itself is a huge mechanical disturbance, much bigger than the disturbances we expect during the pre-seismic time. So it should, and probably does, produce large SEMS from all the mechanisms we have discussed. But the magnitude of these signals decreases as an inverse power of the distance and at 10 km or more from the focal region it should be negligible in most cases. That is why "global" models, which suppose that the source of SEM anomalies is at the earthquake origin, have to introduce some additional (and sometimes unrealistic) suppositions to explain how the signal can still be detected at several hundred kilometers from the focus. Even with these suppositions, the experimental fact is that no SEMS are observed during a quake.

F. Some general recommendations for field experiments can be made based on the model described here. Since all sources should be close to the detector to be observed, the placement of detectors is critical and depends on the frequency range and on whether an electric or magnetic measurement will be made. For example, the nearby presence of rock containing titano-magnetite is required for monitoring tectono-magnetic variation. The existence of a nearby water-saturated layer provides a necessary condition for electrotelluric anomalies as well as geomagnetic variation in the ULF and quasi-static ranges. The best condition for the appearance of anomalies in the RF range is the nearby presence of quartzite or granitic rock and, for their detection, a low crustal conductivity about the detector is also necessary. Because all sources become active only under a mechanical disturbance, the presence of an active geophysical structure such as a fault is necessary.

Since magnetic variation from an electrokinetic source can apear only in the presence of a vertical inhomogeneity, the detector should be placed close to it. For monitoring an electrotelluric anomaly the best setting of the electrodes is across the vertical plane defining the inhomogeneity. The anomaly is enhanced if the water table is close to the surface, provided the electrode separation is not much less than the depth of the table. An electrotelluric anomaly can also be observed without a vertical inhomogeneity if the electrodes are displaced vertically, with one above the water table and the other below it.

Since ULF and RF anomalies are expected to have a pulse-like character, impulse averaging is the best technique for monitoring them. This technique avoids the dead time between impulses, and requires a small acquisition time. On the other hand, the acquisition time should be large enough to record the entire impulse (or a cluster of multiple impulses). The choice of optimal threshold value is also important for this type of averaging, since it should be low enough to record small impulses but high enough for a good signal-to-noise ratio. Following the above recommendations would involve investigating, at the detector location, both the composition of the crust and the noise level in the frequency range of interest.

G. Since our results indicate that SEMS arise from a local source, the usual triangulation technique cannot be used to locate a distant seismic focus. At the heart of our model, however, earthquakes and SEMS are connected by a global stress field. This connectedness means that the possibility still exists for locating a seismic focus using SES. One way is by statistical analysis of these two types of events (SES and earthquakes) using a detector network [*Varotsos et al.,* 1996a, 1996b]. Such an analysis may allow one to establish a connection between a group of SES measurement points and a group of seismic areas.

H. EM emission is a secondary effect of local changes in the stress field of the crust. The question arises, why not measure the stress changes directly? After all, it is known that the latter can be measured with more accuracy. There is at least a twofold answer to why measurements of EME can be useful and can give additional (and sometimes the only) information about stress changes. First, EME measurements can give information about remote stress field changes, while direct stress field measurement give information only at the immediate vicinity of the detector. Second, the latter type of measurement is usually more expensive than EME detection.

Acknowledgments. The authors would like to thank their colleagues Paul J. Wolfe, Kostas Eftaxias and Nikos Bogris for several helpful conversations. Special thanks go to Ms. Barbara O'Brien for typing the manuscript. This research was supported in part by NATO Grant CRG970028.

References

Banos, Jr., A., *Dipole Radiation in the Presence of Conducting Half-Space,* 245 pp., Pergamon, Oxford, 1966.

Bernard, P., Plausibility of long distance electrotelluric precursors to earthquakes, *J. Geophys. Res., 97,* (B12), 17,531–17,546, 1992.

Bishop, J. R., Piezoelectric effects in quartz-rich rocks, *Tectonophysics, 77,* 297–321, 1981.

Biot, M. S., Theory of propagation of elastic waves in a fluid-saturated porous solid, 1. Low frequency range, *Journal of the Acoustical Society of America, 28,* 168–178, 1956.

Breiner, S., Piezomagnetic effect at the time of local earthquakes, *Nature, 202,* 68–69, 1964.

Carmichael, R. S., ed., CRC Practical handbook of physical properties of rocks and minerals, *CRC press, Inc,* 741 pp., 1989.

Chmyrev, V. M., V. N. Isaev, S. V. Bilichenko, and G. Stanev, Observation by space-borne detectors of electric fields and hydromagnetic waves in the ionosphere of an earthquake zone, *Phys. Earth Planetary Interiors, 110,* 1989.

Cress, G. O., B. T. Brady, and A. A. Rowell, Source of electromagnetic radiation from fracture of rock samples in the laboratory, *Geophys. Res. Lett., 14,* (4), 331–334, 1987.

Derr, J., Earthquake's lights: A review of observational and present theories, *Bull. Seismol. Soc. Am., 63,* 2177–2187, 1973.

Deryagin, B. V., N. A. Krotova, and V. P. Smilga, *Adhesion in Solids,* Nauka, Moscow, 1973 (in Russian).

Dobrovolsky, I. P., *The theory of preparation of a tectonic earthquake,* 219 pp., IFZ Akad. Nauk SSSR, Moscow, 1991 (in Russian).

Dobrovolsky, I. P., N. I. Gershenzon, and M. B. Gokhberg, Theory of Electrokinetic Effects Occurring at the Final State in the Preparation of a Tectonic Earthquake, *Physics of the Earth and Planetary Interiors, 57,* 144–156, 1989.

Dobrovolsky, I. P., S. I. Zubkov, and V. I. Myachkin, Estimation of the size of earthquake preparation zones, *Pure Appl. Geophys., 117,* (5), 1025–1044, 1979.

Draganov, A. B., U. S. Inan, and Yu. N. Taranenko, ULF magnetic signature at the Earth surface due to ground water flow: A possible precursor to earthquake, *Geophys. Res. Lett., 18,* 1127–1130, 1991.

Edwards, R. N., The magnetometric resistivity method and its application to the mapping of a fault, *Can. J. Earth Sci., 11,* 1136–1156, 1975.

Eftaxias, K., J. Kopanas, N. Bogris, P. Kapiris, G. Antonopoulos and P. Varotsos, Detection of electromagnetic earthquake precursory signals in Greece, *Proc. Japan Acad., 76(B),* 45–50, 2000.

Eftaxias, K., P. Kapiris, J. Polygiannakis, N. Bogris, J. Kopanas, G. Antonopoulos, A. Peratzakis, and V. Hadjicontis, Signatures of Pending Earthquake from Electromagnetic Anomalies, *Geophys. Res. Lett., 28,* (17), p. 3321, 2001.

Eleman, F., The response of magnetic instruments to earthquake waves, *J. Geomagn. Geoelectr., 18,* (1), 43–72, 1965.

Fenoglio, M. A., M. J. S. Johnston, and J. D. Byerlee, Magnetic and electric fields associated with changes in high pore pressure in fault zones; application to the Loma Prieta ULF emissions, *J. Geophys. Res., 100,* 12,951–12,958, 1995.

Finkel, V. M., Yu. I. Tyalin, and Yu. I. Golovin, Electrization of alkali-haloid crystals during fracture, *Solid State Phys., 21,* 1943–1947, 1985.

Fitterman, D. V., Electrokinetic and magnetic anomalies associated with dilatant regions in a layered earth, *J. Geophys. Res., 83,* (B12), 5923–5928, 1978.

Fitterman, D. V., Theory of electrokinetic-magnetic anomalies in a faulted half-space, *J. Geophys. Res., 84,* (B12), 6031–6040, 1979a.

Fitterman, D. V., Calculations of self-potential anomalies near vertical contacts, *Geophysics, 44,* 1995-2005, 1979b.

Fitterman, D. V., Correction to "Theory of electrokinetic-magnetic anomalies in a faulted half-space", *J. Geophys. Res., 86,* 9585–9588, 1981.

Fraser-Smith, A. C., A. Bernardi, P. R. McGill, M. E. Ladd, R. A. Helliwell, and O. G. Villard, Jr., Low-frequency magnetic field measurements near the epicenter of the Ms 7.1 Loma Prieta earthquake, *Geophys. Res. Lett., 17,* 1465, 1990.

Frenkel, A. I., On the theory of seismic and seismoelectrical phenomena on water-saturated rocks, *Izv., Acad. Sci., USSR, Ser. Geogr. Geophys., 8,* 134–150, 1944.

Fujinawa, Y., and K. Takahashi, Emission of Electromagnetic radiation preceding the Ito seismic swarm of 1989, *Nature, 347,* 376–378, 1990.

Fujinawa, Y., and K. Takahashi, Electromagnetic radiations associated with major earthquakes, *Physics of the Earth and Planetary Interiors, 105,* 249–259, 1998.

Fujinawa, Y., K. Takahashi, T. Matsumoto, and N. Kawakami, Experiments to locate sources of earthquakes-related VLF-electromagnetic signals, *Proc. Japan. Acad., 73(B),* (3), 33–38, 1997.

Fukutomi, T., Report of the Strong Izu earthquake of March 21, 1934, *Bull. Earthq. Res. Inst., Univ. Tokyo, XII,* (3), 527–538, 1934.

Gershenzon, N. I., Seismoelectromagnetic field of electrokinetic nature, *Izvestiya Russia Akademii Nauk, Earth Physics, 28,* (7), 589–596, 1992.

Gershenzon, N. I., and M. B. Gokhberg, On the origin of electrotelluric disturbances prior to earthquakes, *EMC 1989, Nagoya, Japan, September 5–10,* Vol. 1, 116–122, 1989.

Gershenzon, N. I., and M. B. Gokhberg, On earthquake precursors in geomagnetic field variations of electrokinetic nature, *Izvestiya Russia Akademii Nauk, Physics of the Solid Earth. 9,* 100–105, 1992.

Gershenzon, N. I., and M. B. Gokhberg, On Origin of the Electrotelluric field Disturbances Prior to an Earthquake in Kalamata, Greece, *Tectonophysics, 224,* 169–174, 1993.

Gershenzon, N. I., and M. B. Gokhberg, On the origin of anomalous ultralow-frequency geomagnetic disturbances prior to the Loma Prieta, California, earthquake, *Physics of the Solid Earth, 30,* (2), 112–118, 1994.

Gershenzon, N. I., D. O. Zilpimiani, P. V. Mandzhgaladze, O. A. Pokhotelov, and Z. T. Chelidze, Electromagnetic Emission of the Crack Top During Rupture of Ionic Crystals, *Dokl. Akad. Nauk SSSR, 288,* (1), 75–78, 1986.

Gershenzon, N. I., M. B. Gokhberg, V. A. Morgunov, and V. N. Nikolaevskiy, Sources of Electromagnetic Emissions Preceding Seismic Events, *Izvestiya Akademii Nauk SSSR, Physics of the Solid Earth, 23,* (2), 96–101, 1987.

Gershenzon, N. I., M. B. Gokhberg, A. V. Karakin, N. V. Petviashvili, and A. L. Rykunov, Modeling the Connection between Earthquake Preparation Processes and Crustal Electromagnetic Emission, *Physics of the Earth and Planetary Interiors, 57,* 129–138, 1989a.

Gershenzon, N. I., M. B. Gokhberg, and I. P. Dobrovol'sky, Computation of Short-Range Earthquake Precursors in Electrotelluric Field, *Izvestiya Akademii Nauk SSSR, Physics of the Solid Earth, 25,* (11), 901–912, 1989b.

Gershenzon, N. I., M. B. Gokhberg, Yu. P. Kurchashov, E. B. Chirkov, V. I. Chernyi, A. V. Drumya, and M. M. Bogorodsky, On the Generation of Electrotelluric Fields by Crustal Geodynamic Processes, *Proceeding of International Wroclaw Symposium on Electromagnetic Compatibility 06.26-29,* Vol. 2, 877–881, 1990.

Gershenzon, N. I., M. B. Gokhberg, and S. L. Yunga, On the Electromagnetic Field of an Earthquake Focus, *Physics of the Earth and Planetary Interiors, 77,* 13–19, 1993.

Gershenzon, N. I., M. B. Gokhberg, and A. V. Gul'yel'mi, Electromagnetic field of seismic pulses, *Physics of the Solid Earth, 29,* (9), 789–194, 1994.

Ghomshei, M. M., and T. L. Templeton, Piezoelectric and a-axes fabric along quartz vein, *Physics of the Earth and Planetary Interiors, 55,* 374–386, 1989.

Gokhberg, M. B., V. A. Morgounov, and E. L. Aronov, On the high-frequency electromagnetic radiation associated with seismic activity, *Dokl. Akad. Nauk SSSR, 248,* (5) 1077–1081, 1979.

Gokhberg, M. B., V. A. Morgounov, T. Yoshino, and I. Tomizawa, Experimental measurement of electromagnetic emissions possibly related to earthquakes in Japan, *J. Geophys. Res., 87,* (B9), 7884–7888, 1982.

Gokhberg, M. B., I. L. Gufel'd, N. I. Gershenzon, and V. A. Pilipenko, Electromagnetic Effects During Rupture of the Earth's Crust, *Izvestiya Akademii Nauk SSSR, Physics of the Solid Earth, 21,* (1), 52–63, 1985.

Gokhberg, M. B., V. A. Morgounov, and I. V. Matveev, On the observation of anomalous electromagnetic emission in the epicentral zone of earthquake, *Izv. AN SSSR, Fiz. Zemli, 8,* 95–97, 1986.

Gokhberg, M. B., V. A. Morgounov, and O. A. Pokhotelov, *Earthquake Prediction: Seismo-electromagnetic phenomena,* 191 pp.,

Gordon and Breach Publishers, 1995.

Grigoryev, A. I., N. I. Gershenzon, and M. B. Gokhberg, Parametric Instability of Water Drops in an Electric Field as a Possible mechanism for Luminous Phenomena Accompanying Earthquakes, *Physics of the Earth and Planetary Interiors, 57,* 139–143, 1989.

Hanjicontis, V., and C. Mavromatou, Laboratory investigation of the electric signals preceding earthquakes, in *A critical review of VAN: Earthquake prediction from seismic electric signals,* ed. Sir J. Lighthill, World Scientific Publishing Co., Singapore, 106–117, 1996.

Hao, J. Q., L. M. Hastie, and F. D. Stacey, Theory of seismomagnetic effect: A reassessment, *Physics of the Earth and Planetary Interiors, 28,* 129–140, 1982.

Hayakawa, M., R. Kawate, O. A. Molchanov, and K. Yumoti, Result of ultra-low-frequency magnetic field measurements during the Guam earthquake of 8 August 1993, *Geophys. Res. Lett., 23,* (3), 241–244, 1996.

Hayakawa, M., and Y. Fujinawa, Electromagnetic Phenomena Related to Earthquake Prediction, *Terra Scientific Publ.,* Tokyo, 677 pp., 1994.

Honkura, Y., and S. Kubo, Local anomaly in magnetic and electric field variations due to a crustal resistivity change associated with tectonic activity, *J. Geomag. Geoelect., 38,* 1001–1014, 1986.

Ishido, T., and H. Mizutani, Experimental and theoretical basis of electrokinetic phenomena in rock-water systems and its application to geophysics, *J. Geophys. Res., 86,* 1763–1775, 1981.

Ivanov, A. G., Effect of electrization of earth layers by elastic waves passing through them, *Comptes Rendus (Doklady) de l'Academic des Sciences de l'URSS, v. 24,* no. 1, pp. 42–45, 1939.

Johnston, M. J. S., Review of magnetic and electric field effects near active faults and volcanoes in the U.S.A., *Phys. Earth Planet. Inter., 57,* 47–63, 1989.

Johnston, M. J. S., Review of electric and magnetic fields accompanying seismic and volcanic activity, *Surveys in Geophysics, 18,* 441–475, 1997.

Johnston, M. J. S., and R. J. Mueller, Seismomagnetic observation during the 8 July 1986 magnitude 5.9 North Palm Springs Earthquake, *Science, 237,* 1201–1203, 1987.

Kanamori, H., A seismologist's view of VAN, in *A critical review of VAN: Earthquake prediction from seismic electric signals,* ed. Sir J. Lighthill, World Scientific Publishing Co., Singapore, 339–345, 1996.

Kalashnikov, A. C., The possible application of magnetometric methods to the question of earthquake indications, *Trudy Geofiz. Inst. Akad. Nauk SSSR, Sb. Statei, 25,* 162–180, 1954.

Kapitsa, S. P., Magnetic properties of eruptive rocks exposed to mechanical stresses, *Izv. Akad. Nauk SSSR, 86,* 521–523, 1955.

Karakin, A. V., On the derivation of averaged equations of motion for a three-component granular medium, *Izv. Akad. Nauk SSSR, Fiz. Zemli (Solid Earth),* (1), 57–66, 1986.

Karakin, A. V., and L. I. Lobkovsky, On derivation of equations for a three-component visco-deformable medium (crust and the asthenosphere), *Izv. Akad. Nauk SSSR, Fiz. Zemli (Solid Earth),* (12), 3–13, 1985.

Kepis, A. W., M. Maxwell, and R. D. Rusell, Field trials of a seismoelectric method for detecting massive sulfides, *Geophysics, 60,* 365–373, 1995.

Kern, J. W., Effect of moderate stresses on directions of thermoremnant magnetization, *J. Geophy. Res., 66,* 3801–3805, 1961.

Khatiashvili, N. G, On the electromagnetic effect from cracking in alkali-halogen crystals and rocks, *Izv. Akad. Nauk SSSR, Fiz. Zemli (Solid Earth),* (9), 13–19, 1984.

Kopytenko, Yu. A., T. G. Matiashvili, P. M. Voronov, E. A. Kopytenko, and O. A. Molchanov, Detection of ultra-low-frequency emissions connected with the Spitak earthquake and its aftershock activity, based on geomagnetic pulsations data at Dusheti and Vardzia observations, *Phys. Earth Planet. Int., 77,* 85–95, 1993.

Kornfeld, M. I., Ion crystal electrization under stress, *Usp. Fiz. Nauk, 116,* 327–339, 1975.

Kostrov B. V., *Mechanics of the origin of tectonic earthquake,* 176 pp., Nauka, Moscow, 1975.

Kuksenko, V. S., A. I. Lyshkov, K. M. Mirzoev, et al., Relation between the sizes of cracks and duration of the seismic energy release, *Dokl. Akad. Nauk SSSR, 264,* (4), 846–848, 1982.

Landau, L. D., and E. M. Lifshitz, *The classical theory of fields,* 3rd revised Eng. Ed., M. Hamermesh, transl., 354 pp., Pergamon, Oxford and Addison-Wesley, Reading, MA, 1971.

Landau, L. D., and E. M. Lifshitz, *Theory of elasticity,* 3rd revised Eng. Ed. J. B. Sykes and W. H. Reid, transl., 187 pp., Pergamon, Oxford and New York, 1986.

Leland, T. L., and W. K. Rivers, Field measurement of the electroseismic response, *Geophysics, 40,* (2), 233–245, 1975.

Lighthill, J., ed., *A critical review of VAN: Earthquake prediction from seismic electric signals,* 376 pp., World Scientific Publishing Co., Singapore, 1996.

Malyshkov, Yu. P., K. B. Jumabaev, T. A. Omurkulov, and V. F. Gordeev, Litosphere process affected on the formation of Earth pulsed electromagnetic field and earthquakes forecasting, *Vulcanol. Seismol., 1,* 92–105, 1998.

Martner, S. T., and N. R. Sparks, The electroseismic effect, *Geophysics, 24,* (2), 297–308, 1959.

Mastov, Sh. R., V. N. Solomatin, and L. V. Yavorovich, The study of landslide deformation by means of pulsed electromagnetic emission measurements, *Engineer. Geol. 2,* 98–102, 1983.

Mastov, Sh. R., R. M. Gold, V. N. Solomatin, and L. V. Yavorovich, The study of fracture processes during landslide evolution by means of electromagnetic emission measurements, *Engineer. Geol. 1,* 68–71, 1984.

Mavlyanov, G. A., V. I. Ulomov, K. N. Abdullabekov, and S. S. Khusamiddinov, A study of the variations in the parameters of natural electromagnetic fields for earthquake prediction purposes, *Uzb. Geol. Zh.,* (5), 11–22, 1979.

Maxwell, M., R. D. Rassell, A. W. Kepic, and K. B. Butler, Electromagnetic responses from seismically excited target, B: Nonpiezoelectric phenomena, *Exploration Geophysics, 23,* 201–208, 1992.

Merzer, M., and S. L. Klemperer, Modeling low-frequency magnetic-field precursors to the Loma Prieta earthquake with precursory increasc in fault-zone conductivity, *Pure appl. geophys., 150,* 217–248, 1997.

Meyer, K., and R. Pirjola, Anomalous electrotelluric residuals prior to a large imminent earthquake, *Tectonophysics, 125,* 371–378, 1986.

Migunov, N. I., G. A. Sobolev, and A. A. Khromov, Natural electromagnetic radiation in seismically active areas, *Izv. Akad. Nauk SSSR, Fiz. Zemli (Solid Earth),* (7), 55–63, 1984.

Miyakoshi, J., Anomalous time variation of the self-potential in the fractured zone of an active fault preceding the earthquake occurrence, *J. Geomagn. Geoelectr., 38,* 1015–1030, 1986.

Mizutani, H., and T. Ishido, A new interpretation of magnetic field variation associated with the Matsushiro earthquakes, *J. Geomagn. Geoelectr., 28,* 179–188, 1976.

Mizutani, H., T. Ishido, T. Yokokura, and S. Ohnishi, Electrokinetic phenomena associated with earthquakes, *Geophys., Res. Lett., 3,* 365–368, 1976.

Molchanov, O. A., and M. Hayakawa, On the generation mechanism of ULF seismogenic electromagnetic emissions, *Physics of the Earth and Planetary Interiors 105,* 201–210, 1998.

Moore, G. W., Magnetic Disturbances Preceding the 1964 Alaska Earthquake, *Nature, 203,* (4944), 518–519, 1964.

Mueller, R. J., and M. J. S. Johnston, Review of magnetic field monitoring near active faults and volcanic calderas in California: 1974–1995, *Physics of the Earth and Planetary Interiors, 105,* 131–144, 1998.

Myachkin, V. I., *The Process of Earthquake Preparation,* 232 pp., Nauka, Moscow, 1978 (in Russian).

Neyshtadt, N. M., Z. V. Mazanova, L. Ya. Benevich, and M. I. Maiko, *Piezoelectric method of exploration (methodological recommendations),* ONTI VITR, Leningrad, 1972.

Nitsan, V., Electromagnetic emission accompanying fracture of quartz-bearing rocks, *Geophys. Res. Lett., 4,* (8), 333–336, 1977.

Noto, H., Some experiments on earth current (II), *Jap. J. Astron. Geophys., X,* (2), 263–303, 1933.

Ogawa, T., K. Oike, and T. Miura, Electromagnetic variations from rocks, *J. Geophys. Res., 90,* 6245–6249, 1985.

Oike, K., and T. Ogawa, Electromagnetic radiations from shallow earthquakes observed in the LF range, *J. Geomagn. Geoelectr., 38,* 1031–1040, 1986.

Oike, K., and H. Yamada, Relation between shallow earthquake and electromagnetic noises in the LF and VLF ranges, in *Electromagnetic Phenomena Related to Earthquake Prediction,* Hayakawa, M., Fujinawa, Y. (Eds.), *Terra Scientific Publ., Tokyo,* 115–130, 1994.

Ozima, M., T. Mory, and H. Takayama, Observation of Earth-potential using telegraphic facilities and analysis with BAYTAP-G, *J. Geomag. Geoelectr., 41,* 945–962, 1989.

Park, S. K., Precursors to earthquakes: seismoelectromagnetic signals, *Surveys in Geophysics, 17,* 493–516, 1996.

Park, S. K., M. J. S. Johnston, T. R. Madden, F. D. Morgan, and H. F. Morrison, Electromagnetic precursors to earthquakes in the ULF band: a review of observations and mechanisms, *Review of Geophysics,* 31, 117–132, 1993.

Parkhomenko, E. I., *Electrification phenomena in rocks, Monographs in Geoscience,* 285 pp., Plenum Press, New York, 1971.

Qian, F., Y. Zhao, T. Xu, Y. Ming, and H. Zhang, A model of an impending-earthquake precursor of geoelectricity triggered by tidal forces, *Physics of the Earth and Planetary Interiors, 65,* 284–297, 1990.

Ralchovsky, Tz., and L. Komarov, The Vranchea earthquake of 31.08.1986 and its possible electrical precursors, *Bulgarian Academy of sciences, 13,* (4), 59–64, 1987.

Raleigh, R., G. Bennet, H. Graig, T. Hangs, P. Molnar, A. Nur, J. Savage, C. Scholz, R. Turner, and F. Wu, Prediction of the Haicheng earthquake, *Trans. Am. Geophys. Union, 58,* 236–272, 1977.

Rikitake, T., *Earthquake Prediction,* 387 pp., Elsevier, Amsterdam, 1976a.

Rikitake, T., Crustal dilatancy and geomagnetic variations of short period, *J. Geomag. Geoelect., 28,* 145–156, 1976b.

Riznichenko, Yu. V., *Source dimensions of crustal earthquakes and the seismic moment,* pp. 9–27, Nauka, Moscow, 1976.

Sadovsky, M. A., and I. L. Nerssesov, Problems of earthquake prediction, *Izv. Akad. Nauk SSSR, Fiz. Zemli (Solid Earth),* (9), 13–29, 1978.

Sadovsky, M. A., G. A. Sobolev, and N. N. Migunov, Changes in the natural radio emission in the Carpathians, *Dokl. Akad. Nauk SSSR, 244,* (2), 318–321, 1979.

Sasai, Y., Application of the elasticity theory of dislocations to tectonomagnetic modeling, *Bull. Earthq. Res. Iust., 55,* 387–447, 1980.

Sasai, Y., Tectonomagnetic modeling on the basis of linear piezomagnetic theory, *Bull. Earthq. Res. Inst., 66,* 585–722, 1991.

Schloessin, H. H., Experiments on the electrification and luminescence of minerals and possible origins of EQLS and sferics, *Ann. Geophys., 3,* (6), 709–720, 1985.

Shapiro, V. A., and K. N. Abdullabekov, Anomalous variations of the geomagnetic field in East Fergana – magnetic precursor of the Alay earthquake with M=7.0 (November 2, 1978), *Geophys. J. R. Astron. Soc., 68,* 1–5, 1982.

Shapiro, V. A., M. Ju. Muminov, T. Kh. Khadzhyev, and K. N. Abdulabekov, Magnetic field variation of crustal origin measured in the Fergana valley of Uzbekistan, reflecting seismotectonic dynamics, *Electromagnetic phenomena related to earthquake prediction,* pp. 43–49, TERRAPUB, Tokyo, Japan, 1994.

Shiratori, K., Notes on the destructive earthquake in Sagami Bay on the First of September, 1923, *Jap. J. Astron. Geophys., 11,* (4), 174–192, 1925.

Skovorodkin, Y. P., L. S. Bezuglaya, and T. V. Guseva, Tectonomagnetic studies in Tadjikistan, *J. Geomag. Geoelectr., 30,* 481–486, 1978.

Slifkin, A dislocation model for seismic electrical signals, in *A critical review of VAN: Earthquake prediction from seismic electric signals,* ed. Sir J. Lighthill, pp. 91–96, World Scientific Publishing Co., Singapore, 1996.

Sobolev, G. A., and V. M. Demin, *Mechanoelectric phenomena in the Earth,* 210 pp., Nauka, Moscow, 1980 (in Russian).

Sobolev, G. A., V. N. Morozov, and N. I. Migunov, Electrotelluric fields and a large earthquake, *Izv. AN SSSR, Fizika Zemli, 1,* 75–80, 1981.

Sobolev, G. A., V. M. Demin, B. B. Narod, and P. Whaite, Test of piezoelectric and pulsed-radio methods for quartz vein and base-metal sulfides prospecting at Giant Yellowknife Mine, N.W.T., and Sullivan Mine, Kimberly, Canada, *Geophysics, 49,* 2178–2185, 1984.

Solomatin, V. N., I. N. Vasiliev, and Sh. R. Mastov, Natural pulse electromagnetic emission measurements in Yalta hydro-tunnel, *Eng. Geol., 5,* 93–98, 1983.

Solomatin, V. N., L. A. Zashinsly, and Sh. R. Mastov, Application of the electromagnetic emission method to the complex study of rock massifs in Crimea, *Fundamentals of Goophysical Monitoring in Rocks,* pp. 27–31, Novosibirsk, 1983.

Sornette, A., and D. Sornette, Earthquake rupture as a critical point: consequences for telluric precursors, *Tectonophysics, 179,* 327–334, 1990.

Stacey, F. D., The seismomagnetic effect, *Pure Appl. Geophys., 58,* (5), 5–22, 1964.

Stacey, F. D., and M. J. S. Johnston, Theory of the piezomagnetic effect in titanomagnetite-bearing rocks, *Pure Appl. Geophys., 97,* 146–155, 1972.

Stepanov, A. W., Uber den mechanismus der plastischen deformation, *Phys. Z. Soviet Union, 4,* 609–627, 1933.

Tate, J., and W. Daily, Evidence of electro-seismic phenomena, *Phys. Earth Planet. Interiors, 57,* 1–10, 1989.

Terada, T., On luminous phenomena accompanying earthquakes, *Bull. Earthquake Res. Inst. Tokyo Univ., 9,* 225, 1931.

Thompson, R. R., The Seismic-electric effect, *Geophysics, 1,* 327–335, 1936.

Thompson, A. H., and G. A. Gist, Geophysical application of electrokinetic conversion, *The leading edge,* 1169–1173, 1993.

Ulomov, V. I., *Light and electrical phenomena during earthquakes, Tashkent earthquake, 26 April 1966,* pp. 122–140, FAN, Tashkent, 1971.

Uyeda, S., Introduction to the VAN method of earthquake prediction, in *A critical review of VAN: Earthquake prediction from seismic electric signal,* pp. 3–28, ed. Sir J. Lighthill, World Scientific Publishing Co., Singapore, 1996.

Uyeda, S., T. Nagao, Y. Orihara, T. Yamaguchi, and I. Takahashi, Geoelectric potential changes: Possible precursors to earthquakes in Japan, *Proc. Natl. Acad. Sci. USA, 97,* Issue 9, 4561–4566, 2000.

Varotsos, P., and K. Alexopoulos, Physical properties of the variation of the electric field of the earth preceding earthquakes, I, *Tectonophysics, 119,* 73–98, 1984a.

Varotsos, P., and K. Alexopoulos, Physical properties of the variation of the electric field of the earth preceding earthquakes, II, *Tectonophysics, 119,* 99–125, 1984b.

Varotsos, P., and K. Alexopoulos, Physical properties of the variations in the electric field of the earth preceding earthquakes, III, *Tectonophysics, 136,* 335–339, 1987.

Varotsos, P., and K. Alexopoulos, *Thermodynamics of point defects and their relation with bulk properties,* 474 pp., North Holland, Amsterdam, 1986a.

Varotsos, P., and K. Alexopoulos, Thermodynamics of Point Defects and their Relation with Bulk Properties, edited by S. Amelinckx, R. Gevers and J. Nihoul, North Holland, Amsterdam, 1986b.

Varotsos, P., K. Alexopoulos, and M. Lazaridou, Latest aspects of earthquake prediction in Greece based on seismic electric signals II, *Tectonophysics, 24,* 1–37, 1993.

Varotsos, P., K. Lazaridou, K. Eftaxias, G. Antonopoulos, J. Makris, and J. Kopanas, Short term earthquake prediction in Greece by seismic electric signals, in *A critical review of VAN: Earthquake prediction from seismic electric signals,* pp. 29–76,

ed. Sir J. Lighthill, World Scientific Publishing Co., Singapore, 1996a.

Varotsos, P., K. Eftaxias, M. Lazaridou, K. Nomicos, N. Sarlis, N. Bogris, J. Makris, G. Antonopoulos, and J. Kopanas, Recent earthquake prediction results based on the observation of seismic electric signals, *Acta Geophysica Polonica, XLVI,* (4), 301–327, 1996b.

Varotsos, P., N. Sarlis, K. Lazaridou, and P. Kapiris, Transmission of stress induced electric signals in dielectric media, *Journal of Applied Physics, 83,* (1), 60–70, 1998.

Volarovich, M. P., G. A. Sobolev, and E. I. Parkhomenko, The piezoelectric effect in pegmatite and quartz veins, *Izzvestiya Acad. Sci. USSR, Geophysics Series,* 145–152, 1962.

Volarovich, M. P., and E. I. Parkhomenko, The piezoelectric effect in rocks, *Izv. AN SSSR, ser. Geophys., 3,* 37–48, 1955.

Vorobyev, A. A., M. A. Samokhvalov, R. N. Ibragimov, and M. T. Usmanova, Searching for effects due to the existence of local large electric fields in the lithosphere, *Seismol. Uzb. Tashkent, FAN,* 213–219, 1975.

Vorobyev, A. A., M. A. Samokhvalov, and A. F. Gorelkin, Anomalous electric field variations prior to the earthquakes near Tashkent, *Uzbek Geol. J.,* (2), 37–41, 1976.

Warwick, J. W., C. Stoker, and T. R. Meyer, Radio emission associated with rock fracture: possible application for the Great Chilean Earthquake of May 22, 1960, *J. Geophys. Res., 87,* (B4), 2851–2859, 1982.

Wolfe, P. J., J. Yu, and N. I. Gershenzon, Seismoelectric studies in an outwash plain, *Proc. Symp. on the Appl. of Geophys. to Eng. and Env. Problems, Wheat Ridge, Col.,* 21–30, 1996.

Yamada, I., K. Masuda, and H. Mizutani, Electromagnetic and acoustic emission associated with rock fracture, *Phys. Earth Planetary Interiors, 57,* 157–168, 1989.

Yusui, I., Luminous phenomena in connection with the Matsushiro earthquake swarm, *Rep. Kakioko Magn. Observ., 4,* 52–60, 1968.

Yoshimatsu, T., The measurements of earth-current potentials and its reliability, *Mem. Kakioka Magn. Obs. Suppl., 1,* 1–29, 1957.

Yoshino, T., and I. Tomizawa, Observation of low-frequency electromagnetic emissions as precursors to the volcanic eruption at Mt. Mihara during November, 1986, *Phys. Earth Planetary Interiors, 32,* 1989.

Zablocki, C. J., Electrical transients observed during underground nuclear explosions, *J. Geophys. Res., 71,* (14), 3523–3542, 1966.

Zhurkov, S. N., V. S. Kuksenko, and V. A. Petrov., On prediction of rock failure, *Izv. Akad. Nauk SSSR, Fiz. Zemli (Solid Earth), 6,* 1977.

Zlotnicki, J., and F. H. C. Cornet, A numerical model of earthquake-induced piezomagnetic anomalies, *J. Geophys. Res., 91,* 709–718, 1986.

Zlotnicki, J., J. P. Pozzi, and F. H. Cornet, Investigation of induced magnetization variations caused by triaxial stresses, *J. Geophys. Res., 86,* (B12), 11899–11909, 1981.

(Received September 21, 2001)

Appendix A

Crustal deformation is accompanied by the process of pore water diffusion. The hydrodynamics of pore water was described in the classic papers of *Frenkel* [1944] and *Biot* [1956]. We can write the following equation describing the relation between the change in volume strain $\theta = \Delta V/V$ and the hydrostatic pressure change P in a porous, water-saturated medium [*Frenkel,* 1944]:

Table A1. Mechanical parameters of water-saturated rock

K_0	2.5×10^{10} Pa
K	$0.5\ K_0$
K_2	$0.1\ K_0$
k_0	10^{-12}–10^{-16} m^2

μ_v	5×10^{-4} Pa-S
μ_s	3×10^{10} Pa
ρ_w	10^3 kg/m^3
ρ_{matrix}	$3\rho_w$
m	0.1

$$\frac{1}{K_2}\frac{\partial^2 P}{\partial t^2} - \frac{\mu_v}{K_2 k_0 \rho_w}\frac{\partial P}{\partial t} - \frac{1}{\beta' \rho_w}\nabla^2 P = = -\frac{\beta - 1}{\beta'}\frac{\partial^2 \theta}{\partial t^2} + \frac{\mu_v \beta}{k_0 \rho_w \beta'}\frac{\partial \theta}{\partial t}\ , \tag{A1}$$

where $\beta = (1 - K/K_0)/m; \beta' = 1 + (\beta - 1)K_2/K_0; K_0, K$ and K_2 are the bulk moduli of rock matrix, dry porous rock, and pore water, respectively; m is the porosity; μ_v, k_0 and ρ_w are the dynamic viscosity, permeability, and density of water, respectively. Note that the magnitude of θ depends in general on P. However, for most rock parameter values, the changes in pore pressure have practically no effect on the volume strain. This is why we shall suppose that θ depends only on time t and position $\vec{r}$, but is independent of P. So $\theta(t, \vec{r})$ acts simply as a source function in Equation A1.

Let's compare the first two terms on the left in Equation A1, assuming a monochromatic disturbance of frequency ω and time dependence $e^{i\omega t}$. Then these terms are $-\omega^2 P/K_2$ and $i\omega\mu_v P/K_2 k_0 \rho_w$. If $\omega \gg \omega_{\text{const}} \equiv \mu_v/k_0\rho_w$ then the second term on the left can be ignored. By a similar argument the second term on the right can be ignored relative to the first term. This means that the pore pressure will be described by the inhomogeneous wave equation,

$$\nabla^2 P - \frac{\beta' \rho_w}{K_2}\frac{\partial^2 P}{\partial t^2} = (\beta - 1)\rho_w \frac{\partial^2 \theta}{\partial t^2}\ . \tag{A2}$$

From this equation we can define the speed of propagation of compressional waves in pore water:

$$V^2_{\text{water}} = \frac{K_2}{\beta' \rho_w}\ . \tag{A3}$$

Compare this speed with the speed of compressional waves in the matrix [*Landau and Lifshitz,* 1986]:

$$V^2_{\text{matrix}} = \frac{3K_0 + 4\mu_s}{3\rho_{\text{matrix}}}\ , \tag{A4}$$

where μ_s is shear modulus and ρ_{matrix} is the density of the matrix. Using typical parameters (Table 6), we find $V^2_{\text{water}}/V^2_{\text{matrix}} \approx 1/10$.

From Equation A2, when a seismic wave of frequency $\omega \gg \omega_{\text{const}}$ and wavelength $\lambda = 2\pi V_{\text{matrix}}/\omega$ propagates through a porous medium, it will drive the pressure fluctuations in the water at the same frequency and wavelength. The second term on the left in Equation A2 is therefore essentially $\omega^2 P/V^2_{\text{water}}$ while the term $\nabla^2 P$ is of order $(2\pi/\lambda)^2 P$ or $\omega^2 P/V^2_{\text{matrix}}$. This latter term will be much smaller than the former; ignoring it gives

$$-\frac{\beta'\rho_w}{K_2}\frac{\partial^2 P}{\partial t^2} \approx (\beta-1)\rho_w\frac{\partial^2\theta}{\partial t^2}\ . \tag{A5}$$

Integration results in

$$P = -\frac{\beta-1}{\beta'}K_2\theta\ . \tag{A6}$$

(Under conditions of hydrostatic equilibrium, the constants of integration vanish.)

Now consider the situation when $\omega \ll \omega_0$. In this case we can neglect the terms in Equation A1 containing the second time derivatives, leading to a diffusion-type equation:

$$\frac{\mu_v}{k_0\rho_w}\frac{\partial p}{\partial t} - \frac{K_2}{\beta'\rho_w}\nabla^2 P = -\frac{\mu_v\beta K_2}{k_0\beta'\rho_w}\frac{\partial\theta}{\partial t}\ . \tag{A7}$$

It is easy to show that, in this case also, the pressure fluctuations will track the volume fluctuations. To see this we again consider a seismic wave as the driving force. The first term on the left is $\mu_v i\omega P/k_0\rho_w$ or $i\omega_{\text{const}}\omega P$, while the second term is essentially $(K_0/\beta'\rho_w)\omega^2 P/V^2_{\text{matrix}}$ or $(V^2_{\text{water}}/V^2_{\text{matrix}})\omega^2 P$. The latter term can be ignored compared to the former, so

$$\frac{\mu_v}{k_0\rho_w}\frac{\partial P}{\partial t} \approx -\frac{\mu_v\beta K_2}{k_0\beta'\rho_w}\frac{\partial\theta}{\partial t}\ . \tag{A8}$$

Therefore

$$P = -\frac{K_2\beta}{\beta'}\theta\ . \tag{A9}$$

So in order to connect P and θ for fast processes when $\omega \gg \omega_{\text{const}}$ we should use Equation A6 and for slow processes (like water diffusion after sudden changes of volume strain) we should use Equation A9.

Appendix B

We present here asymptotic formulas for the components of the above-ground electromagnetic field produced by horizontal and vertical electric and magnetic dipoles embedded in the conducting half-space $z > 0$ (see Figure 2a in Section 4) with conductivity σ, electric permeability ε and magnetic susceptibility μ [*Banos,* 1966]. The distance r from the coordinate origin is characterized as being in the near zone, intermediate zone or far zone (see Section 4 and Figure 2b). In order to save space, we present results only for the dominant components in the intermediate and far zones. For the near zone, all components are given. The quantities n, k_1 and k_2 are defined in Section 4.

1. Horizontal electric dipole

(a) Near zone

$$E_r \cong \frac{P\cos\varphi}{2\pi\sigma r^3}\exp[ik_1 h] \tag{B1}$$

$$E_\varphi \cong \frac{P\sin\varphi}{\pi\sigma r^3}\exp[ik_1 h] \tag{B2}$$

$$E_z \cong -\frac{ik_1 P\cos\varphi}{2\pi\sigma r^2}\exp[ik_1 h] \tag{B3}$$

$$H_r \cong \frac{iP\sin\varphi}{\pi k_1 r^3}\exp[ik_1 h] \tag{B4}$$

$$H_\varphi \cong -\frac{iP\cos\varphi}{2\pi k_1 r^3}\exp[ik_1 h] \tag{B5}$$

$$H_z \cong -\frac{3P\sin\varphi}{2\pi k_1^2 r^4}\exp[ik_1 h] \tag{B6}$$

(b) Intermediate zone

$$E_z \cong -\frac{k_2^2 P\cos\varphi}{2\pi\sigma r}\frac{1}{n}\exp[ik_2 r + ik_1 h] \tag{B7}$$

$$H_\varphi \cong \frac{ink_2 P\cos\varphi}{2\pi r}\exp[ik_2 r + ik_1 h] \tag{B8}$$

(c) Far zone

$$E_z \cong -\frac{ik_1 P\cos\varphi}{2\pi\sigma n^2 r^2}\exp[ik_2 r + ik_1 h] \tag{B9}$$

$$H_\varphi \cong -\frac{P\cos\varphi}{2\pi n r^2}\exp[ik_2 r + ik_1 h] \tag{B10}$$

2. Horizontal magnetic dipole

(a) Near zone

$$E_r \approx \frac{iMk_1\sin\varphi}{2\pi\sigma r^3}\exp[ik_1 h] \tag{B11}$$

$$E_\varphi \cong -\frac{iMk_1\cos\varphi}{2\pi\sigma r^3}\exp[ik_1 h] \tag{B12}$$

$$E_z \cong -\frac{Mk_1^2\sin\varphi}{2\pi\sigma r^2}\exp[ik_1 h] \tag{B13}$$

$$H_r \cong \frac{M\cos\varphi}{\pi r^3}\exp[ik_1 h] \tag{B14}$$

$$H_\varphi \cong \frac{M\sin\varphi}{2\pi r^3}\exp[ik_1 h] \tag{B15}$$

$$H_z \cong \frac{3iM\cos\varphi}{2\pi k_1 r^4}\exp[ik_1 h] \tag{B16}$$

(b) Intermediate zone

$$E_z \cong -\frac{iMk_1k_2^2\sin\varphi}{2\pi\sigma r}\frac{1}{n}\exp[ik_2r+ik_1h] \quad \text{(B17)}$$

$$H_\varphi \sim -\frac{Mk_2^2\sin\varphi}{2\pi r}\exp[ik_2r+ik_1h] \quad \text{(B18)}$$

(c) Far zone

$$E_z \cong \frac{Mk_1^2\sin\varphi}{2\pi\sigma n^2r^2}\exp[ik_2r+ik_1h] \quad \text{(B19)}$$

$$H_\varphi \cong -\frac{iMk_1\sin\varphi}{2\pi nr^2}\exp[ik_2r+ik_1h] \quad \text{(B20)}$$

3. Vertical electric dipole
(a) Near zone

$$E_r \cong \frac{ink_2P}{2\pi\sigma r^2}\exp[ik_1h] \quad \text{(B21)}$$

$$E_z \cong -\frac{P\exp[ik_1h]}{2\pi\sigma r^3} \quad \text{(B22)}$$

$$H_\varphi \cong \frac{Pn^2\exp[ik_1h]}{2\pi r^2} \quad \text{(B23)}$$

(b) Intermediate zone

$$E_z \cong \frac{k_2^2P}{2\pi\sigma r}\exp[ik_2r+ik_1h] \quad \text{(B24)}$$

$$H_\varphi \cong -\frac{in^2k^2P}{2\pi r}\exp[ik_2r+ik_1h] \quad \text{(B25)}$$

(c) Far zone

$$E_z \cong \frac{ik_1P}{2\pi\sigma nr^2}\exp[ik_2r+ik_1h] \quad \text{(B26)}$$

$$H_\varphi \cong \frac{P}{2\pi r^2}\exp[ik_2r+ik_1h] \quad \text{(B27)}$$

4. Vertical magnetic dipole
(a) Near zone

$$H_r \cong -\frac{nM(3+2ik_2r)}{2\pi r^3}\exp[ik_1h] \quad \text{(B28)}$$

$$H_z \cong -\frac{n^2M(4+3ik_2r)}{2\pi r^3}\exp[ik_1h] \quad \text{(B29)}$$

$$E_\varphi \cong -\frac{iMk_2(3+2ik_2r)}{2\pi\sigma r^3}\exp[ik_1h] \quad \text{(B30)}$$

(b) Intermediate and far zones

$$H_r \cong \frac{ink_2M}{2\pi r^2}\exp[ik_2r+ik_1h] \quad \text{(B31)}$$

$$E_\varphi \cong \frac{k_2^2M}{2\pi\sigma r^2}\exp[ik_2r+ik_1h] \quad \text{(B32)}$$

Appendix C

In Section 4, consideration of the electrokinetic effect resulted in Equation 21b, in which the second and third terms involve surface integrals instead of volume integrals. To see how this comes about, consider the volume integral (see Equation 12),

$$\vec{I} = \int\limits_V \vec{j}^{\,0}dV = \int\limits_V \sigma C\nabla P dV$$

where $\vec{j}^{\,0}$ is the electrokinetic current and the integral is over the crust. If the crust is homogeneous this integral equals zero, since P is a localized function, i.e. vanishes at large distances. Now suppose there is an inhomogeneity across the plane x=0, resulting in a discontinuity in the coefficient $C : C = C_1H(x) - C_2H(-x)$. Then

$$\vec{I} = \iiint\limits_\infty \sigma\Big[C_1H(x) - C_2H(-x)\Big] \times$$

$$\times \left[\hat{i}\frac{\partial P}{\partial x} + \hat{j}\frac{\partial P}{\partial y} + \hat{k}\frac{\partial P}{\partial z}\right]dxdydz =$$

$$= \hat{i}(C_1 - C_2)\sigma\int\limits_S P(r,t)dS\ .$$

If $P(r,t) \approx P(0)\frac{l_c}{r}\exp\left[-\frac{r}{L} - \left(\frac{t-r/V}{\Delta t}\right)^2\right]H(r - l_c)$, $\vec{I}$ can be written in the form

$$\vec{I} = \hat{i}\sigma(C_1 - C_2)l_c^2\int\limits_S \frac{l_c}{r}\exp\Big[-\frac{r}{L} -$$

$$- \left(\frac{t-r/V}{\Delta t}\right)^2\Big]H(r-l_c)dS/l_c^2 =$$

$$= \vec{P}_K\int\limits_S \frac{l_c}{r}\exp\left[-\frac{r}{L} - \left(\frac{t-r/V}{\Delta t}\right)^2\right]H(r-l_c)dS/l_c^2\ ,$$

which is the second term in Equation 21b. The same reasoning can be applied to the third term.